

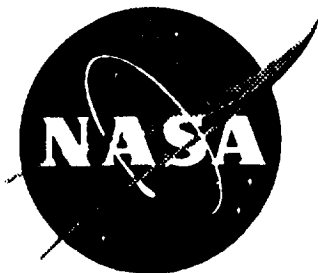
NASA TECHNICAL MEMORANDUM 109052

N-24
203596
67P

**Analysis of Local Delaminations Caused by Angle Ply
Matrix Cracks**

Satish A. Salpekar, T. Kevin O'Brien and K. N. Shivakumar

November 1993



**National Aeronautics and
Space Administration**

**LANGLEY RESEARCH CENTER
Hampton, Virginia 23681-0001**

(NASA-TM-109052) ANALYSIS OF LOCAL
DELAMINATIONS CAUSED BY ANGLE PLY
MATRIX CRACKS (NASA) 67 P

N94-24083

Unclass

G3/24 0203596

SUMMARY

Two different families of graphite/epoxy laminates with similar layups but different stacking sequences, $(0/\theta/-\theta)_S$ and $(-\theta/\theta/0)_S$, were analyzed using three-dimensional finite element analysis for $\theta = 15$ and 30 degrees.

Delaminations were modeled in the $-\theta/\theta$ interface, bounded by a matrix crack and the stress free edge. The total strain energy release rate, G , along the delamination front was computed using three different techniques: the virtual crack closure technique (VCCT), the equivalent domain integral (EDI) technique, and a global energy balance technique. The opening fracture mode component of the strain energy release rate, G_I , along the delamination front was also computed for various delamination lengths using VCCT. The effect of residual thermal and moisture stresses on G was evaluated.

KEYWORDS: Composite Material, Graphite Epoxy, Delamination, Matrix Crack, Finite Element Analysis

INTRODUCTION

The design of composite structural parts and their life prediction under service conditions requires the understanding of the details of damage modes occurring in composites [1]. Some of the important damage modes in laminated composites are matrix cracking and the local delamination in the region where a matrix crack meets a stress free edge. Such local delaminations may contribute to eventual failure of the laminate.

The tests conducted on $[0_n/\pm 15]_s$ laminates by Lagace and Brewer [2] showed that the delamination area in the 15/-15 interface extended between the transverse ply crack and the free edge. O'Brien & Hooper [3] and O'Brien [4] found that matrix cracking was detected as the first event, followed by local delamination, in $(0_2/\theta_2/-\theta_2)_s$ graphite/epoxy laminates ($\theta=20, 25, 30$ degrees) subjected to tension fatigue loading. This same damage sequence was observed by O'Brien [5] in $(\theta_2/-\theta_2/0_2)_s$ graphite/epoxy laminates ($\theta=15, 30$ degrees). The matrix cracks formed near the stress free edge and the local delaminations formed in the $\theta/-\theta$ interface. These local delaminations were bounded between the free edge and the matrix crack, as shown schematically in figure 1.

Salpekar and O'Brien [6] analyzed $(0/\theta/-\theta)_s$ graphite/epoxy laminate ($\theta=15, 45$ degrees) subjected to tension load, using a three-dimensional finite element analysis. For the $\theta=15$ degree case, the matrix cracking in the -15 ply was found to create a very large, and possibly singular, interlaminar tension stress in the 15/-15 interface. This apparent singularity indicated that the delamination may initiate at the point where the matrix crack intersects the laminate edge. For the $\theta=45$ degree case, the strain energy release rate, G ,

for a local delamination was calculated for a delamination in the 45/-45 interface, growing uniformly away from the matrix crack in the -45 degree ply. For this case, G was higher near the laminate edge than in the interior of the laminate. In an experimental and analytical study, Fish and O'Brien [7] concluded that in $(15/90_n/-15)_s$ glass/epoxy laminates, the interlaminar tensile stresses due to cracking in the +15 degree ply plays a significant role in the onset of local delamination.

The purpose of the present study was to compute the strain energy release rates associated with local delaminations originating from matrix cracks in two different families of laminates with similar layups but different stacking sequences. Both $(0/\theta/-\theta)_s$ and $(-\theta/\theta/0)_s$ graphite/epoxy laminates were analyzed using three-dimensional finite element analysis, for $\theta = 15$ and 30 degrees. These two cases were chosen because they bound the behavior observed in experiments on orthotropic laminates with angle ply matrix cracks [3-5]. The experimentally observed local delaminations that formed in the $-\theta/\theta$ interface and were bounded by the matrix crack and the stress free edge were modeled using three-dimensional finite elements. The strain energy release rate, G , along the delamination front was computed using three different techniques; the virtual crack closure technique (VCCT) [8], the equivalent domain integral (EDI) technique [9-11], and a global energy balance technique [12]. The computation of G was performed for three delamination fronts corresponding to three unique delamination lengths. The effect of residual thermal and moisture stresses on G was also evaluated.

LAMINATE CONFIGURATIONS AND LOADING

The two graphite/epoxy laminates, $(0_2/\theta_2/-\theta_2)_s$ and $(\theta_2/-\theta_2/0_2)_s$, tested in references 3-5 were 5 inches long, 1 inch wide, and 12 plies thick, each ply being .005 inches thick. For simplicity in the modeling, these laminates were assumed to be 6 plies thick, with each ply having a thickness of 0.01 inches. Furthermore, in order to take advantage of symmetry in boundary conditions, the second stacking sequence was altered in the modeling so that the $-\theta$ degree ply was on the surface. Hence, the two laminates were modeled as $(0/\theta/-\theta)_s$ and $(-\theta/\theta/0)_s$ laminates.

Because the matrix cracks and local delaminations observed in references 3-5 never extended a distance greater than 5 to 10 times the ply thickness (h) from the free edge, for reasons of computational efficiency specimen dimensions were assumed in the model that were much smaller than the physical dimensions. As shown in fig.2, the model was $75h$ long by $10h$ wide. The coordinate axes were assumed as shown in the fig. 2, with the origin located at point A. Only half of the laminate thickness was modeled and the symmetry boundary conditions were applied on the appropriate plane of symmetry for each stacking sequence. Thus, the symmetry condition was applied on the $z=0$ plane for $(0/\theta/-\theta)_s$ laminate, and on the $z=3h$ plane for the $(-\theta/\theta/0)_s$ laminate.

The matrix crack extended through the thickness of the $-\theta$ degree ply, parallel to the fiber direction in the xy plane. Although the matrix cracks observed at the free edge in references 3-5 formed at oblique angles to the xy plane (fig.1), the matrix crack plane was modeled normal to the xy plane for simplicity and computational efficiency (fig.2).

The local delamination was modeled in the $\theta/-\theta$ interface, with the delamination front inclined at an angle of 2θ to the free edge as observed in references 3-5 (fig. 1). The elastic constants for the graphite/epoxy material used in the analysis are shown in Table 1. The laminate was subjected to a uniform displacement by constraining the plane $x=0$ in the x direction and by applying an arbitrary uniform displacement of 0.01 inch in the positive x -direction to the $x=75h$ plane (fig. 2). This displacement corresponded to a uniform axial strain of 0.0133 in/in. Residual thermal and hygroscopic loads were applied as described in reference 13.

ANALYSIS

The finite element model of the laminate consisted of 2394 20-noded hexahedral elements having 11,560 nodes (fig. 3). A fine mesh was used in the area surrounding the intersection of the $-\theta$ degree matrix ply crack and the free edge. For elements at the intersection of the matrix crack and free edge, the nodes on two edges of the hexahedral elements were consolidated to form pentahedral elements.

The region of local delamination in the $\theta/-\theta$ interface bounded between the matrix crack and the free edge was modeled beginning with the first delamination front at a distance of one ply thickness, h , from the intersection of the matrix crack with the free edge, followed by elements one third of a ply thickness, $h/3$, long at the free edge (fig. 4). All elements had a z -direction thickness of $h/3$. This mesh was gradually transitioned to a coarser mesh away from the region of local delamination. Separate finite element models were generated for $\theta = 15$ and $\theta = 30$ degrees cases for the two layups $(0/\theta/-\theta)_S$ and $(-\theta/\theta/0)_S$. Separate models were needed for each θ because the matrix

crack in the $-\theta$ degree ply was parallel to the fiber direction and the delamination front in the xy plane was inclined at 2θ to the free edge (fig. 1).

The strain energy release rate associated with the local delamination was calculated at the delamination front which was inclined at 2θ to the free edge (fig.1). Three different delamination fronts were used for the G calculation. The length, a , of the delamination front measured along the free edge for the three cases, was $1.66h$, $2.33h$, and $3.33h$, where h is the ply thickness. The delamination front was subdivided into six equal length, L , segments as shown in fig. 4. The magnitude of L for any particular front was a function of the delamination length, a , and θ .

Because the in-plane normal stresses perpendicular to the fiber direction, σ_{22} , in the $-\theta$ degree ply had been previously determined to be tensile only near the free edge [3], G calculations were performed for two different damage configurations. In the first case, the matrix crack was modeled at a distance corresponding to the length at which the matrix crack faces started to cross into one another. The matrix crack length, d , was then held fixed and the delaminations were extended to compute G . The delamination front never reached the matrix crack front in this case. In the second case, the matrix crack extended only as far as the delamination front for each increment of delamination growth.

Three different methods were used to compute G . The first method was based on the change in the global energy due to the movement of the delamination front and gives the average G between two delamination fronts [12]. The other two methods, the Virtual Crack Closure Technique (VCCT) and the Equivalent Domain Integral (EDI) technique, were used to compute the distribution of G along the delamination front at each delamination length.

The VCCT is well documented in the literature [8]. The VCCT techniques requires that the elements behind and ahead of the delamination front be orthogonal to the delamination front. In the present problem, this requirement is violated because the finite element mesh configuration is dictated by the shape of the local delamination. The local delamination initiates at the intersection of the matrix crack in the $-\theta$ ply and the free edge and the delamination front is inclined at 2θ to the free edge. Thus, the finite element mesh will appear to be radiating from a corner as shown in figure 3. The EDI technique [9,10,11] does not have this orthogonality requirement. Therefore, the G computation was alternatively performed using EDI, and the results of the two methods were compared.

The EDI method is used to obtain the total J-integral for cracked elastic and elastic-plastic bodies. For an elastic body, J is equivalent to G. The total J-integral at any point along the crack front in a 3-D cracked body is defined as an integral of the energy potential over a closed surface around the crack front. Recently, the surface integral was extended to a volume integral, called the equivalent domain integral, for ease of implementation in a finite-element analysis and accurate evaluation of the integral [9,10,11]. This was done using Green's divergence theorem and de Lorenzi's s-function [14]. The s-function is a continuous function defined from the inner surface to the outer surface of the domain selected for the J-integral calculation. The J-integral is evaluated from the accumulated stress-work density, stress, total strain, and displacement fields.

To implement the EDI method, element numbers are input within the user selected domain, at node numbers on the inner surface at which s is defined to be 1. The selection of the domain depends on the gradient of the strength of singularity along the crack front, and the finite element modeling in the crack

front region, etc. The guidelines for the selection of the s-function and the domain are given in reference 11.

TOTAL G RESULTS AND DISCUSSION

The results of the analysis of $(0/\theta/-\theta)_S$ and $(-\theta/\theta/0)_S$ graphite/epoxy laminates for $\theta = 15$ and 30 degrees are discussed. For each layup, the G results are presented for a fixed matrix ply crack length ahead of the delamination front as well as for the case where the matrix ply crack extends only as far as the delamination front. The effect of delamination growth was studied by considering three delamination lengths ($a/h = 1.66, 2.33, 3.33$). The effect of thermal and moisture residual stresses on the $(0/30/-30)_S$ laminate was also analyzed (see appendix).

Results for $(0/15/-15)_S$ Laminates

The matrix ply crack in the -15 ply was allowed to grow in $h/3$ increments until the crack faces began crossing into one another. This crack length was found to be $d=3.67h$. Then, keeping this crack length constant, the delamination was modeled considering three delamination lengths ($a/h = 1.66, 2.33, 3.33$).

The strain energy release rate along the delamination front for each case is shown in figures 5-7, respectively. The results from the VCCT and EDI methods agree well along the middle of the delamination front but diverge near the matrix crack and the free edge where the EDI values were always lower than the VCCT values. The difference in the VCCT and EDI results are limited to the last element near the matrix crack and the free edge. If a more refined

mesh had been used, with more elements along the delamination front, the difference in the two techniques for calculating G would be insignificant everywhere except at the matrix crack and free edge. Hence, the VCCT technique yields accurate G distributions along the delamination front even though the finite element mesh at the delamination front is not orthogonal.

The VCCT results for all three delamination fronts are shown in figure 8. The G distribution is relatively uniform along the front at $a/h=1.66$, but becomes slightly skewed at $a/h=3.33$, with a greater G near the free edge than near the matrix crack. This change in the G distribution indicates that the delamination may change shape slightly as it grows, deviating from the 2θ angle with the free edge that was originally assumed.

The average G along the front calculated using the VCCT and EDI techniques was obtained for each delamination length. These average G values are plotted in figure 9. As noted previously, the average EDI values are lower than the VCCT values, but this discrepancy would diminish if a more refined mesh was used near the matrix crack and free edge. Also shown in figure 9 are the average G values between successive delamination fronts, obtained from the change in global energy, and plotted at the midpoint between the fronts. The first point from the "global energy" method ($a=1.33h$) corresponds to the average energy released from the initial delamination length modeled at $a=1.0h$ up to the first delamination front at $a=1.66h$. The average G increases slightly with increasing a/h and the VCCT and global energy based methods are in good agreement. Although the assumption of orthogonality is violated in the modeling, VCCT gives fairly accurate results, which are in agreement with the global energy balance. Therefore, VCCT appears to be a robust technique for G calculation.

The G variations along the delamination front for the three values of a/h where the matrix crack extends only to the delamination front are shown in figure 10. The average G calculated using VCCT along the front as a function of a/h is shown in figure 11. Also shown in figure 11 is the average G calculated using VCCT along the front vs. a/h from figure 9. The average G where the matrix crack extends only as far as the delamination front is lower than the average G where the matrix crack length is held constant at $d=3.67h$. Hence, the matrix crack length will influence the magnitude of the strain energy release rate for local delamination growth. A corresponding G analysis for matrix crack growth would need to be performed and compared to an appropriate failure criteria to establish which case is more appropriate. Such an analysis may need to be performed iteratively with the delamination analysis because any delamination that initiates may also influence the G for further matrix crack growth. However, experimental observations for brittle matrix composites [3-5] indicates that the assumption made in the first case, of a constant matrix crack length corresponding to the distance to crack closure, may be a reasonable approximation for analyzing delamination onset and assessing delamination durability.

Results for (0/30/-30)_S Laminate

In the analysis of (0/30/-30)_S laminate, the matrix ply crack was grown up to $d=4.33h$ before the crack faces started crossing into one another. This crack length was then held constant and the G computation was performed for local delamination growth. Figures 12-14 show the G variation across the delamination front, for $a/h=1.66, 2.33, 3.33$, respectively. As noted previously, the EDI results agree with the VCCT results along the middle of the

delamination front but diverge for the elements near the matrix crack and the free edge where the EDI values were lower than the VCCT values. However, G values calculated in the middle of the delamination front using these two techniques for $a/h=1.66$ (fig.12) do not agree as closely as was observed for the longer delamination lengths (figs.13&14).

Figure 15 shows the VCCT results for the three values of a/h . The G distribution are slightly skewed for all three values of a/h , with a greater G near the free edge than near the matrix crack. The distributions become less uniform with increasing a/h . This skewness in the G distribution indicates that the original delamination shape may deviate from the 2θ angle originally assumed and that the delamination may change shape as it grows.

The average G across the front, as calculated by VCCT as a function of a/h , is shown in figure 16. The variation in G with increasing a/h is fairly small, with a only a slight decrease in G up to $a/h=3.33$. Similar to the $\theta=15$ degree case, the VCCT and the global energy method are in good agreement and the EDI values are lower due to the lower values in the end segments.

The G variations along the delamination front for the three values of a/h where the matrix crack extends only to the delamination front are shown in figure 17. The average G along the front as a function of a/h is shown in figure 18. Also shown in figure 18 is the average G along the front vs. a/h from figure 16. As noted previously for the $\theta=15$ degree case, the average G where the matrix crack extends only as far as the delamination front is lower than the average G where the matrix crack length is held constant at $d=4.33h$. Hence, the matrix crack length will influence the magnitude of the strain energy release rate for local delamination growth.

Results for (-15/15/0)_s Laminate

For the (-15/15/0)_s layup, the matrix crack length in the -15 degree ply was maintained at $d=3.67h$; the same length as the (0/15/-15) layup. G was also computed for the same delamination locations; $a/h=1.66, 2.33, 3.33$. The G distributions along the delamination front are shown in figures 19-21. The comparison between EDI and VCCT is consistent with the previous layup. However, G values calculated in the middle of the delamination front using these two techniques for $a/h=1.66$ (fig.19) do not agree as closely as was observed in the previous layups or as was observed for the longer delamination lengths for this layup (figs.20&21).

Figure 22 compares VCCT G distributions along the delamination front for all three delamination lengths. The G distributions are skewed for all three values of a/h . Unlike the previous cases, however, the distributions are more non-uniform at the smaller delamination lengths, indicating that the original delamination shape may deviate significantly from the 2θ angle originally assumed but may approach this shape as the delamination grows.

The average G across the delamination front, as a function of a/h , is shown in figure 23. The variation is fairly small, with a slight decrease in G , up to $a/h=3.33$. As noted previously, the VCCT and the global energy method are in good agreement and the EDI values are lower due to the lower values in the end segments.

Results for (- 30/30/0)_s Laminate

For the (-30/30/0)_s layup, the matrix crack length in the -30 ply was maintained at $d=4.33h$; the same length as the (0/30/-30) layup. Figures 24 and

25 show the G distribution along the delamination front for the $(-30/30/0)_S$ layup containing a matrix crack in the -30 ply, for $a/h=1.66$ and 3.33 , respectively. The comparison between EDI and VCCT is consistent with the previous layup. As noted in that case, G values calculated in the middle of the delamination front using these two techniques for $a/h=1.66$ (fig.24) do not agree as closely they did for the longer delamination length of $a/h=4.33$ (fig.25).

Figure 26 compares VCCT G distributions along the delamination front for all three delamination lengths. The G distributions are skewed for all three values of a/h . The distribution at the intermediate delamination length ($a/h=2.33$) is the most uniform, indicating that the original delamination shape may deviate from the 2θ angle originally assumed, but the delamination approaches this shape before deviating once again with further growth.

The average G across the delamination front, as a function of a/h , is shown in figure 27. There is a slight decrease in G with delamination length up to $a/h=3.33$. As noted previously, the VCCT and the global energy method are in good agreement and the EDI values are lower due to the lower values in the end segments.

Comparison of 15 and 30 degree layups

Figures 28 and 29 compare the average G along the delamination front for the 15 and 30 degree layups for the two unique stacking sequences, respectively. For both stacking sequences, the 30 degree layup had a greater average total G than the 15 degree layup.

G_I RESULTS AND DISCUSSION

Recent studies have indicated that G components due to the three unique fracture modes I, II, and III (corresponding to opening, sliding shear, and tearing shear, respectively), as calculated using the VCCT technique in finite element analyses, are dependent on the mesh refinement at the delamination front [15-17]. This mesh size dependence has been attributed to the oscillatory nature of the singularity associated with a crack growing at a bimaterial interface [16]. Two techniques have been proposed to overcome this limitation. The first involves modeling the resin rich layer between delaminating plies as a thin adhesive film and simulating the delamination growth within this thin resin layer. Although this technique yields G components that are independent of mesh refinement, it requires a very fine mesh near the delamination front, and greatly increases the number of degrees of freedom required in the model. The second technique involves modifying specific material properties in the elements at the delamination front such that the oscillatory term in the singularity vanishes [17]. This technique has only recently been proposed, and to date, has not been attempted in fully 3D analyses.

These techniques are needed if a quantitative comparison of calculated fracture modes are required to compare to delamination failure criteria for predicting experimentally observed delamination failures. However, if a reasonable mesh refinement is used at the delamination front, where element dimensions are no larger than the ply thickness, h , and no smaller than the fiber tow dimensions (typically $h/20$ for graphite fiber reinforced composites), qualitative conclusions may be drawn as to the presence and distribution of the three fracture modes for delamination in a particular laminate configuration and loading. This is the approach that was taken in the present study.

The opening fracture mode component of the strain energy release rate, G_I , was determined using the VCCT technique for the cases where the matrix crack length was held constant. However, because of the non-orthogonality of the finite element mesh, the two independent shear fracture mode components, G_{II} and G_{III} could not be isolated. However, the sum of these two modes must equal the difference in the total G and the mode one component, G_I . In addition, for brittle epoxy matrix composites, the mode I interlaminar fracture toughness, G_{Ic} , is typically much lower than either the mode II or mode III interlaminar fracture toughness, G_{IIc} and G_{IIIc} , respectively [3-5]. Hence, The presence of mode I, and its relative contribution to total G , is often of primary concern.

Results for $\theta = 15$ degree Laminates

Figures 30 and 31 show the distribution of G_I across the delamination front for the $(0/15/-15)_S$ and $(-15/15/0)_S$ laminates, respectively. For all three delamination lengths modeled, the mode I component was greatest near the matrix crack and vanished near the free edge. In addition, the mode I component decreased with increasing delamination length. Fig. 32 shows the dependence of G_I on delamination length using the value calculated next to the matrix crack for both laminates. Fig. 33 shows the ratio of G_I to the total G as a function of delamination length using the values calculated next to the matrix crack for both laminates. Comparison of the $(0/15/-15)_S$ and $(-15/15/0)_S$ laminates in figures 32 and 33 illustrate the influence of stacking sequence on local delamination. The G_I/G ratio for the $(-15/15/0)_S$ laminate with a matrix crack in the surface -15 degree ply is greater

than the G_I/G ratio for the $(0/15/-15)_S$ laminate with a matrix crack in the -15 degree ply in the interior of the specimen thickness.

Results for $\theta = 30$ degree Laminate

Figures 34 and 35 show the distribution of G_I across the delamination front for the $(0/30/-30)_S$ and $(-30/30/0)_S$ laminates, respectively. For all three delamination lengths modeled, the mode I component was greatest near the matrix crack and decreased near the free edge. In addition, the mode I component decreased with increasing delamination length. Fig. 36 shows the dependence of G_I on delamination length using the value calculated next to the matrix crack for both laminates. Fig. 37 shows the ratio of G_I to the total G as a function of delamination length using the values calculated next to the matrix crack for both laminates. Comparison of the $(0/30/-30)_S$ and $(-30/30/0)_S$ laminates in figures 36 and 37 illustrate the influence of stacking sequence on local delamination. The G_I/G ratio for the $(-30/30/0)_S$ laminate with a matrix crack in the surface -30 degree ply is greater than the G_I/G ratio for the $(0/30/-30)_S$ laminate with a matrix crack in the -30 degree ply in the interior of the specimen thickness.

Comparison of 15 and 30 degree layups

Figures 38 and 39 compare the G_I/G ratios for the 15 and 30 degree layups for the two unique stacking sequences, respectively. For both stacking sequences, the 30 degree layup had a greater G_I/G ratio than the 15 degree layup.

CONCLUSIONS

Two different families of graphite/epoxy laminates with similar layups but different stacking sequences, $(0/\theta/-\theta)_s$ and $(-\theta/\theta/0)_s$, were analyzed using three-dimensional finite element analysis for $\theta = 15$ and 30 degrees.

Delaminations were modeled in the $-\theta/\theta$ interface, bounded by a matrix crack and the stress free edge. The total strain energy release rate, G , along the delamination front was computed using three different techniques: the virtual crack closure technique (VCCT), the equivalent domain integral (EDI) technique, and a global energy balance technique. The opening fracture mode component of the strain energy release rate, G_I , along the delamination front was also computed for various delamination lengths using VCCT. The effect of residual thermal and moisture stresses on G was evaluated. From these analyses, the following conclusions were drawn:

- (1) The variation of average G along the delamination front as a function of delamination length was relatively small, with the VCCT and global energy based methods showing good agreement.
- (2) The G distributions along the delamination front calculated from the VCCT and EDI methods agree well in the interior but diverge at the end segments near the matrix crack and the free edge. The EDI values at the end segments were always lower than the VCCT values. The average EDI values were lower than the values obtained by the other two methods due to the significantly lower G values at the end segments.

(3) Although the assumption of orthogonality is violated in the finite element model, VCCT gives fairly accurate results, which are in agreement with the global energy balance and EDI techniques. Therefore, VCCT appears to be a robust technique for G calculation.

(4) The matrix crack length influences the magnitude of the G for delamination. For both layups analyzed, the average G along the delamination front for the case where the matrix crack extends with the delamination front was lower than the average G for the case where the matrix crack was a constant length beyond the delamination front.

(5) For both layups modeled, the opening mode, G_I , was greatest near the matrix crack and decreased near the free edge. In addition, G_I decreased with increasing delamination length. The laminates that had a matrix crack in the surface ply had a greater G_I/G ratio than the laminates that had a matrix crack in the interior of the specimen thickness.

(6) The addition of the contribution of thermal residual stresses, resulting from the cool down after cure, to the strain energy released as the delamination grows results in a G^{M+T} value that is greater than G^M for mechanical loading only. The subsequent addition of moisture relaxes these residual thermal stresses, and hence, decreases G^{M+T+H} .

APPENDIX

EFFECTS OF THERMAL AND MOISTURE STRESSES

The effect of residual thermal stresses, due to the difference in cure and room temperature, and hygroscopic stresses, due to moisture weight gain, on the value of G was also analyzed for the $[0/30/-30]_S$ laminate. In addition to the uniform mechanical axial strain (ϵ), the laminate was subjected to a temperature drop (ΔT) and an increase in humidity (ΔH). The coefficients of thermal expansion and moisture absorption used in the analysis are shown in Table 1. Figures 40-42 show the G along the delamination front due to the combined mechanical, thermal, and hygroscopic loadings for a matrix crack length of $4.33h$ and a delamination length of $3.33h$. Results are shown for: (1) the same mechanical loading, ϵ , applied previously, but with $\Delta T = -280^\circ\text{F}$ and $\Delta H = 0.0\%$ (fig.40); this same ϵ but with $\Delta T = -280^\circ\text{F}$ and $\Delta H = 0.6\%$ (fig.41); and this same ϵ but with $\Delta T = -280^\circ\text{F}$ and $\Delta H = 1.2\%$ (fig.42). As in the previous cases, the EDI and VCCT agree well in the middle of the delamination front but diverge at the ends, with the agreement being best for the longer delamination lengths. Figure 43 shows the effect of the different loadings on G calculated from the elements closest to the free edge. G^M corresponds to mechanical load only, whereas G^{M+T} corresponds to mechanical plus thermal loading only. The additional contribution of the thermal residual stresses (resulting from the cool down after cure) to the strain energy released as the delamination grows results in a G^{M+T} value that is greater than G^M for mechanical loading only. The subsequent additional moisture contribution relaxes these residual thermal stresses, and hence, decreases G as shown by the two other loading cases designated G^{M+T+H} .

REFERENCES

1. O'Brien, T.K., "Towards a Damage Tolerance Philosophy for Composite Materials and Structures, " *Composite Materials: Testing and Design*. ASTM STP 1059, 1990, p.7-33.
2. Lagace, P.A., and Brewer, J.C., "Studies of Delamination Growth and Final Failure under Tensile Loading, " *ICCM VI. London, Vol. 5. Proceedings*, July 1987, pp. 262-273.
3. O'Brien, T.K., and Hooper, S.J., "Local Delamination in Laminates with Angle Ply matrix Cracks, Part I: Tension Tests and Stress Analysis, " *Composite Materials: Fatigue and Fracture, 4th Volume*, ASTM STP 1156, June 1993, pp. 507-537.
4. O'Brien, T.K., "Local Delamination in Laminates with angle Ply Matrix Cracks, Part II: Delamination Fracture Analysis and Fatigue Characterization," *Composite Materials: Fatigue and Fracture, 4th Volume*. ASTM STP 1156, June 1993, pp. 538-551.
5. O'Brien, T.K. , "Stacking Sequence Effect on Local Delamination Onset in Fatigue , " *Proceedings of the International Conference on Composite Materials*. Wollongong, Australia, Feb. 1993.
6. Salpekar, S.A., and O'Brien, T.K. , "Analysis of Matrix Cracking and Local Delamination in $(0/0/-0)_S$ Graphite Epoxy Laminates under Tension Load, "

ASTM Journal of Composites Technology and Research, Vol. 15, No. 2,
Summer, 1993, pp. 95 - 100.

7. Fish, J.C., and O'Brien, T.K., "Three-Dimensional Finite Element Analysis of Delamination from Matrix cracks in Glass-Epoxy Laminates, " *Composite Materials: Testing and Design. 10th Vol.* ASTM STP 1120, 1992. pp. 348-364.
8. Rybicki, E.F. , and Kanninen, M.F., "A Finite-Element Calculation of stress Intensity Factors by Modified Crack Closure Integral, " *Engng. Fract. Mech.*, Vol. 9, 1977, pp. 931-938.
9. Nikishkov, G.P., and Atluri, S.N., "Calculation of Fracture Mechanics Parameters for an Arbitrary Three-Dimensional Crack by the 'Equivalent Domain Integral' Method, " *Int. J. Numer. Methods in Engng.*, Vol. 24, 1987, pp. 1801-1821.
10. Shivakumar, K.N., Tan, P.W., and Newman, J.C. , Jr., "A Virtual Crack Closure Technique for Calculating Stress-Intensity Factors for Cracked Three-Dimensional Bodies," *Int. J. Fract.*, Vol. 36, 1988, pp. R43-R50.
11. Shivakumar, K. N. , and Raju, I. S. , "A Three-Dimensional Equivalent Domain Integral for Mixed Mode Fracture Problems," *NASA CR-182021*, 1990.
12. Salpekar, S.A. , Raju, I. S. , and O'Brien, T.K., "Strain-Energy-Release Rate Analysis of Delamination in a Tapered Laminate Subjected to Tension

- Load," *Journal of Composite Materials*, Vol. 25, February 1991, pp.118-141.
13. O'Brien, T.K. , "Residual Thermal and Moisture Influences on the Analysis of Local Delaminations," *ASTM Journal of Composites Technology and Research*, Vol. 14, No. 2, Summer, 1992, pp.86-94.
 14. de Lorenzi, H.G. , "On Energy Release Rate and the J-Integral for 3-D Crack Configuration," *Int. J. Fracture*, Vol. 19, 1982, pp. 183-192.
 15. Sun, C.T., and Monoharan, M.G., "Strain Energy Release Rate of an Interface Crack Between Two Orthotropic Solids," Proceedings of the American Society for Composites, Second Technical Conference, Technomic Pub. Co., Lancaster, Sept. 1987, pp.49-57.
 16. Raju, I.S., Crews, J.H., Jr., and Aminpour, M.A., "Convergence of Strain Energy Release Rate Components for Edge-delaminated Composite Laminates," *Engng. Frac. Mech.*, Vol.30, 1988, pp.383-396.
 17. Davidson, B., "Prediction of Energy Release Rate for Edge Delamination using a Crack Tip element," Presented at the Fifth ASTM Symposium on Composite Materials: Fatigue and Fracture, Atlanta, GA, May, 1993.

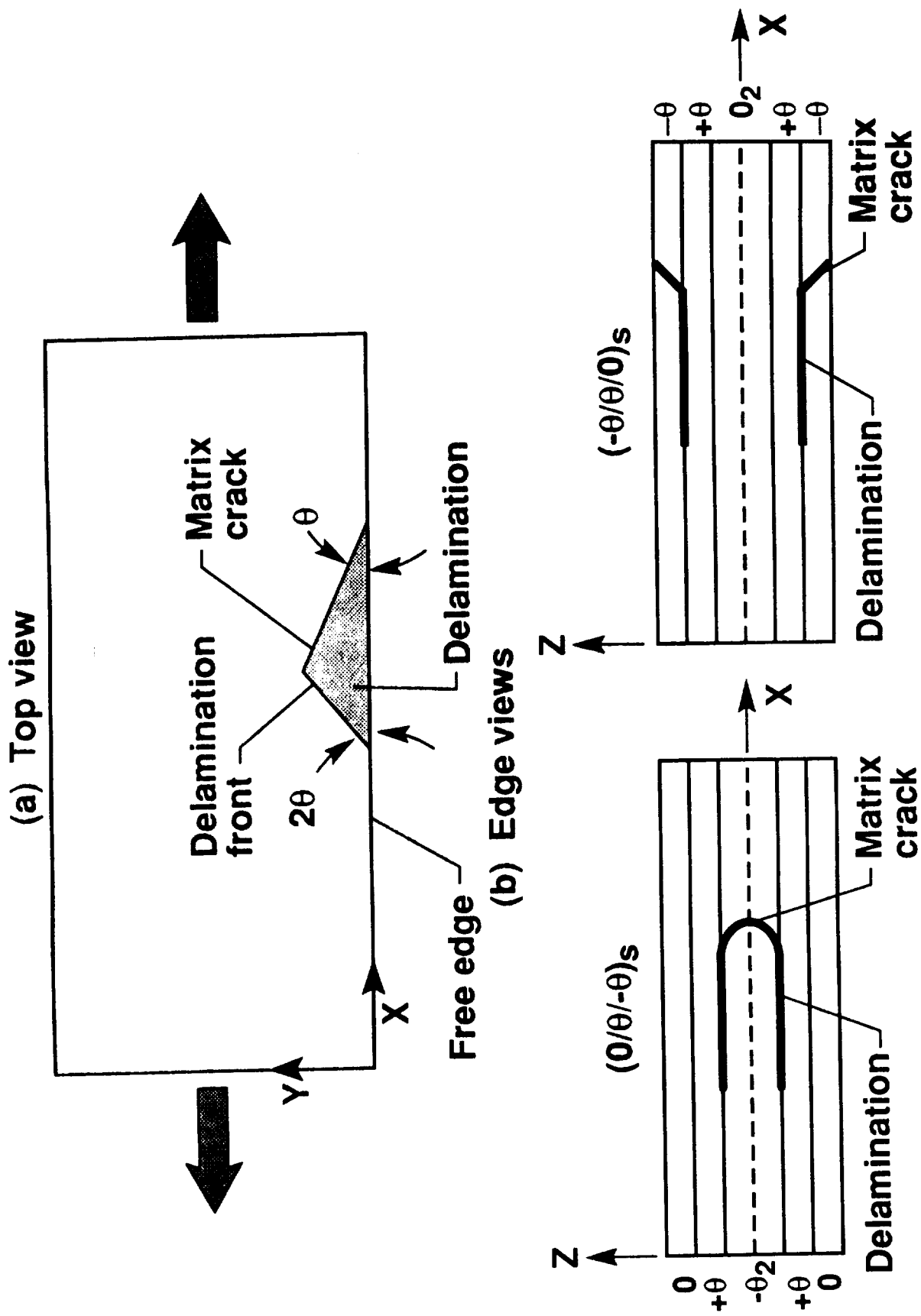


Fig. 1 Schematic of matrix crack induced local delamination

Note:
Drawing
not to scale

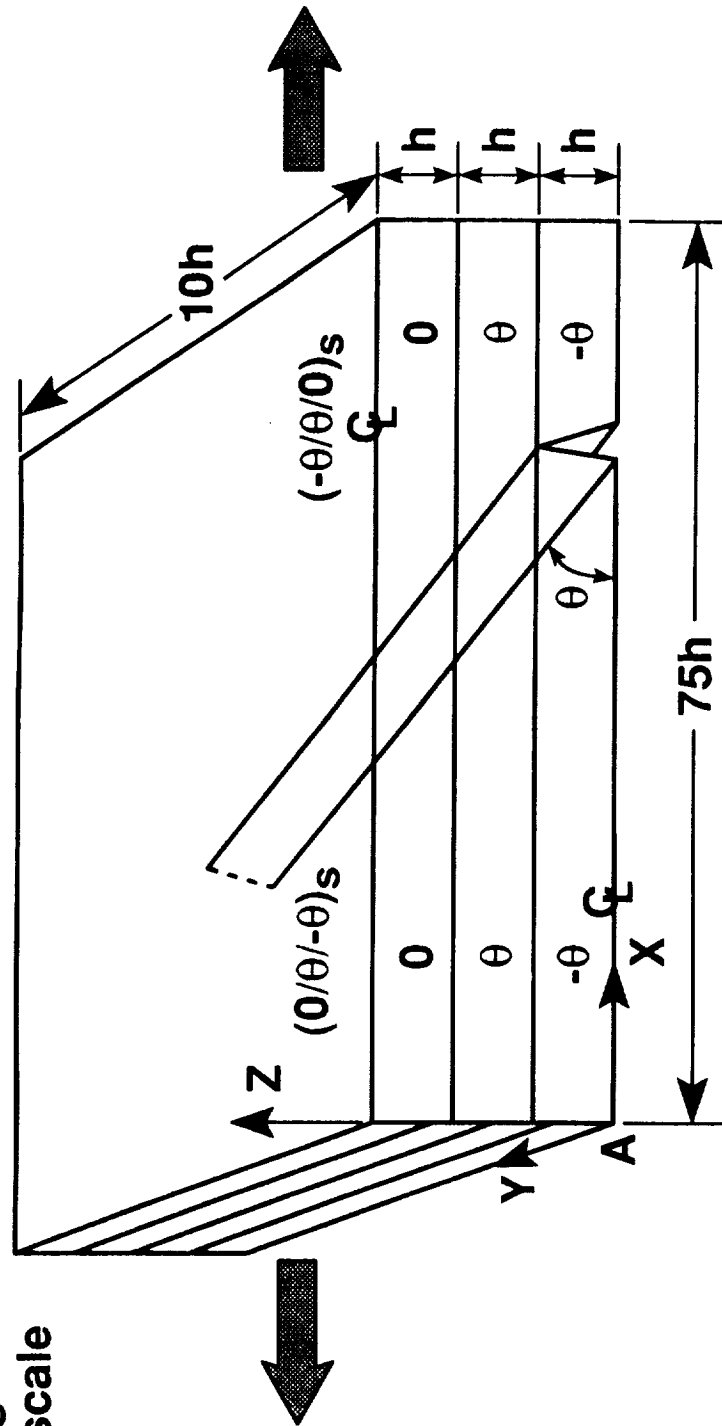


Fig. 2 Symmetry conditions for laminate stacking sequences modeled

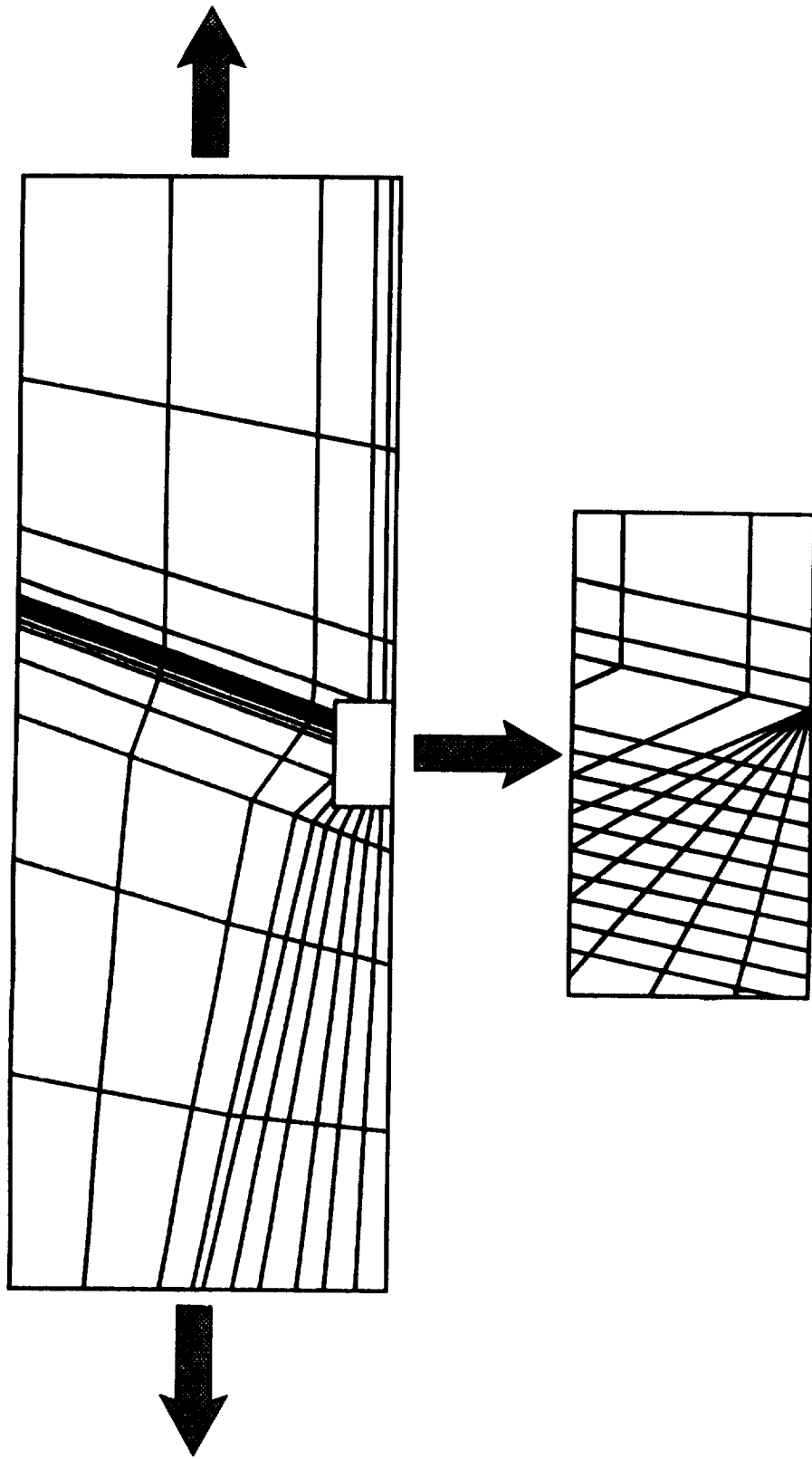


Fig. 3 View of finite element mesh in the xy plane

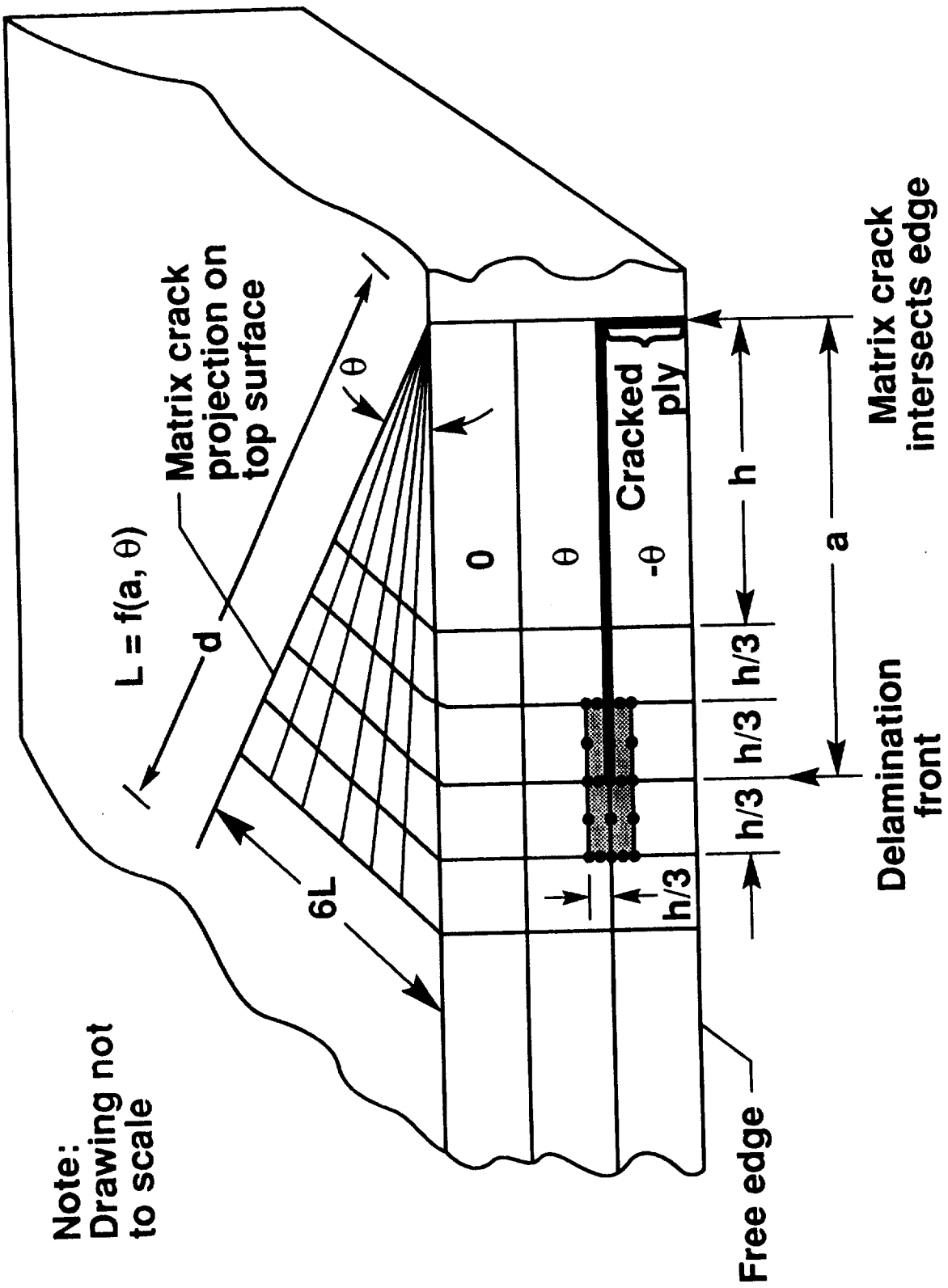


Fig. 4 Schematic showing local details of finite element mesh

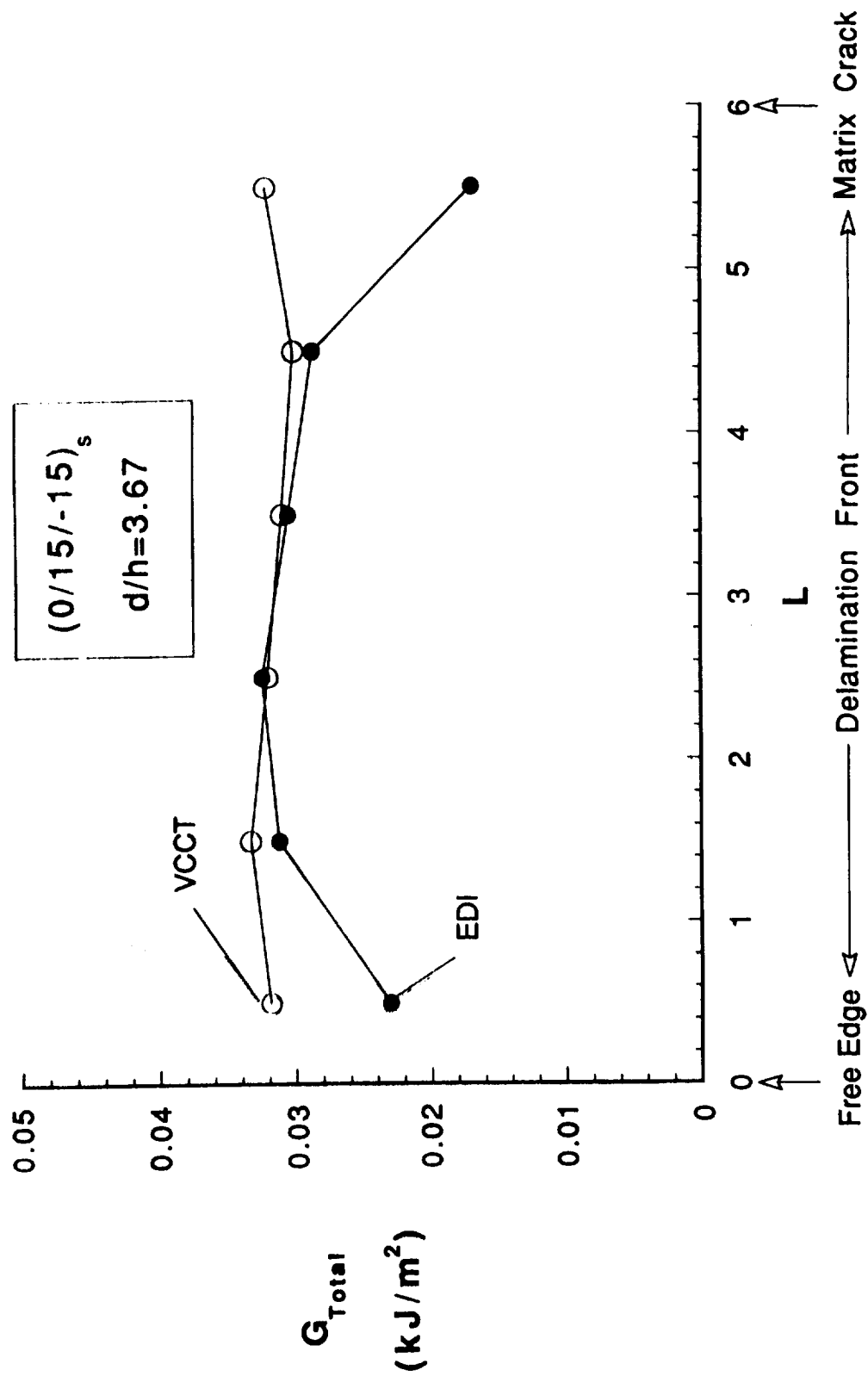


Fig.5 G Distribution Along Delamination Front in $(0/15/-15)_s$ laminate for $a/h=1.66$

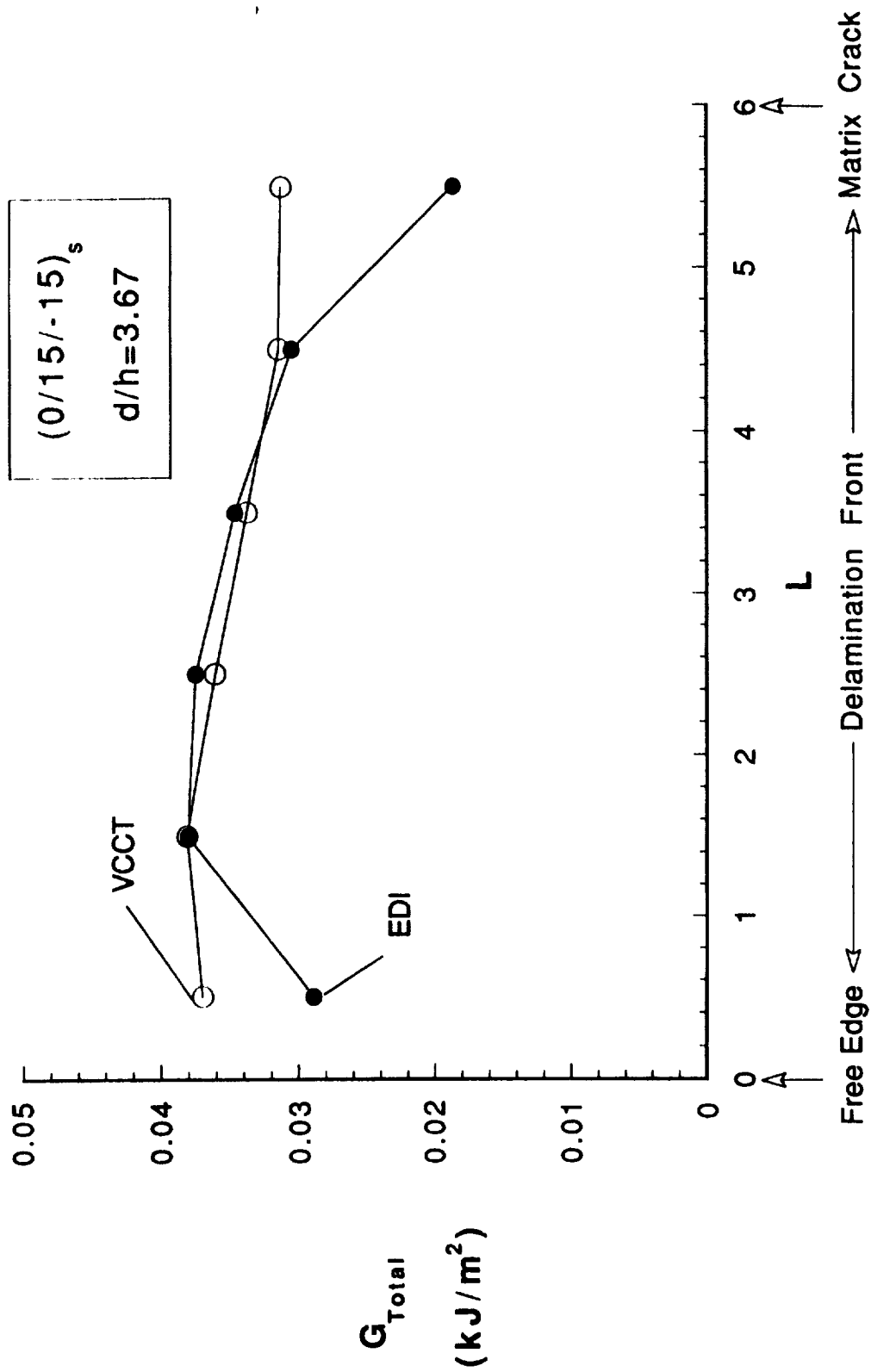


Fig.6 G Distribution Along Delamination Front in $(0/15/-15)_s$ laminate for $a/h=2.33$

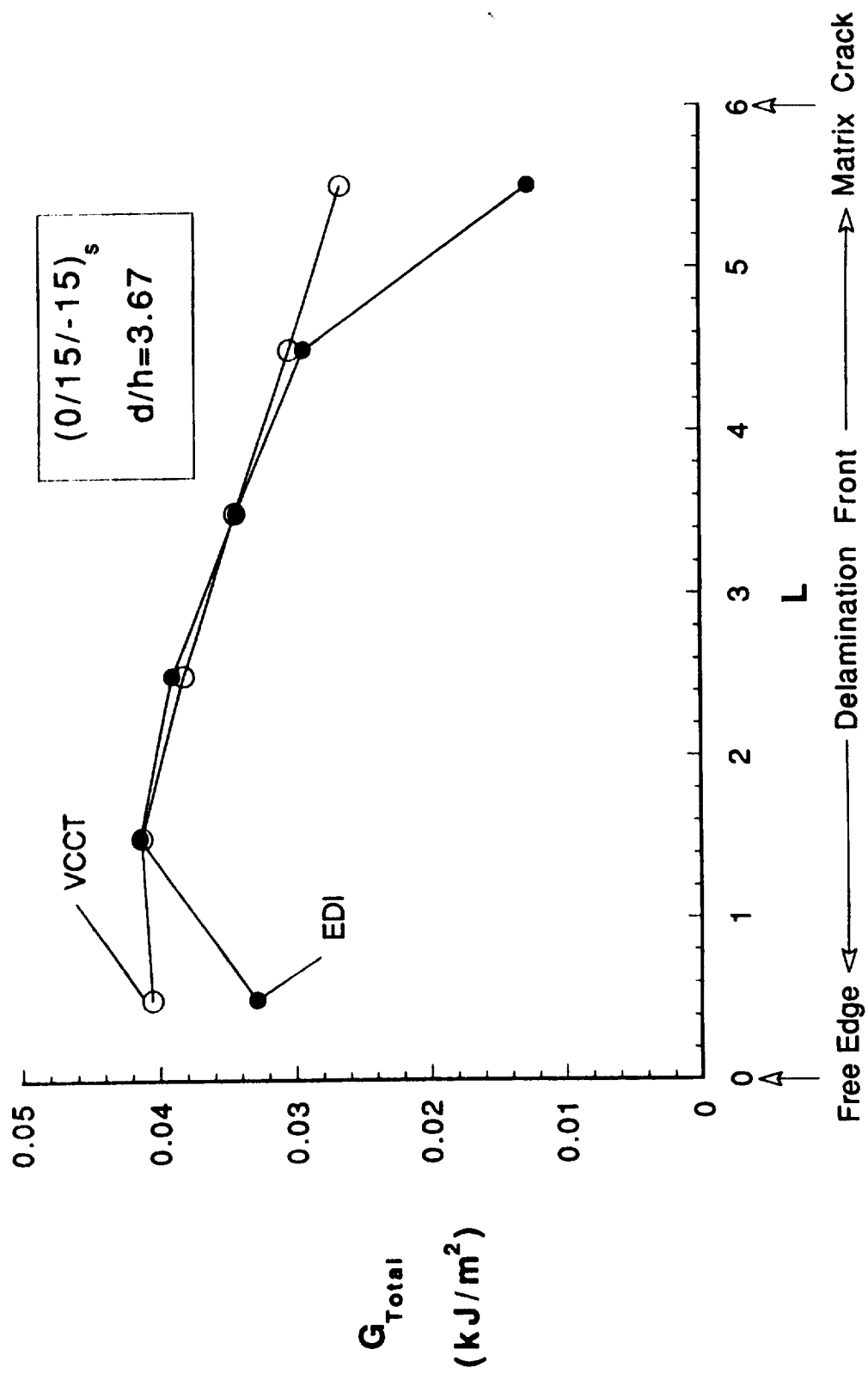


Fig.7 G Distribution Along Delamination Front in $(0/15/-15)_s$ laminate for $a/h=3.33$

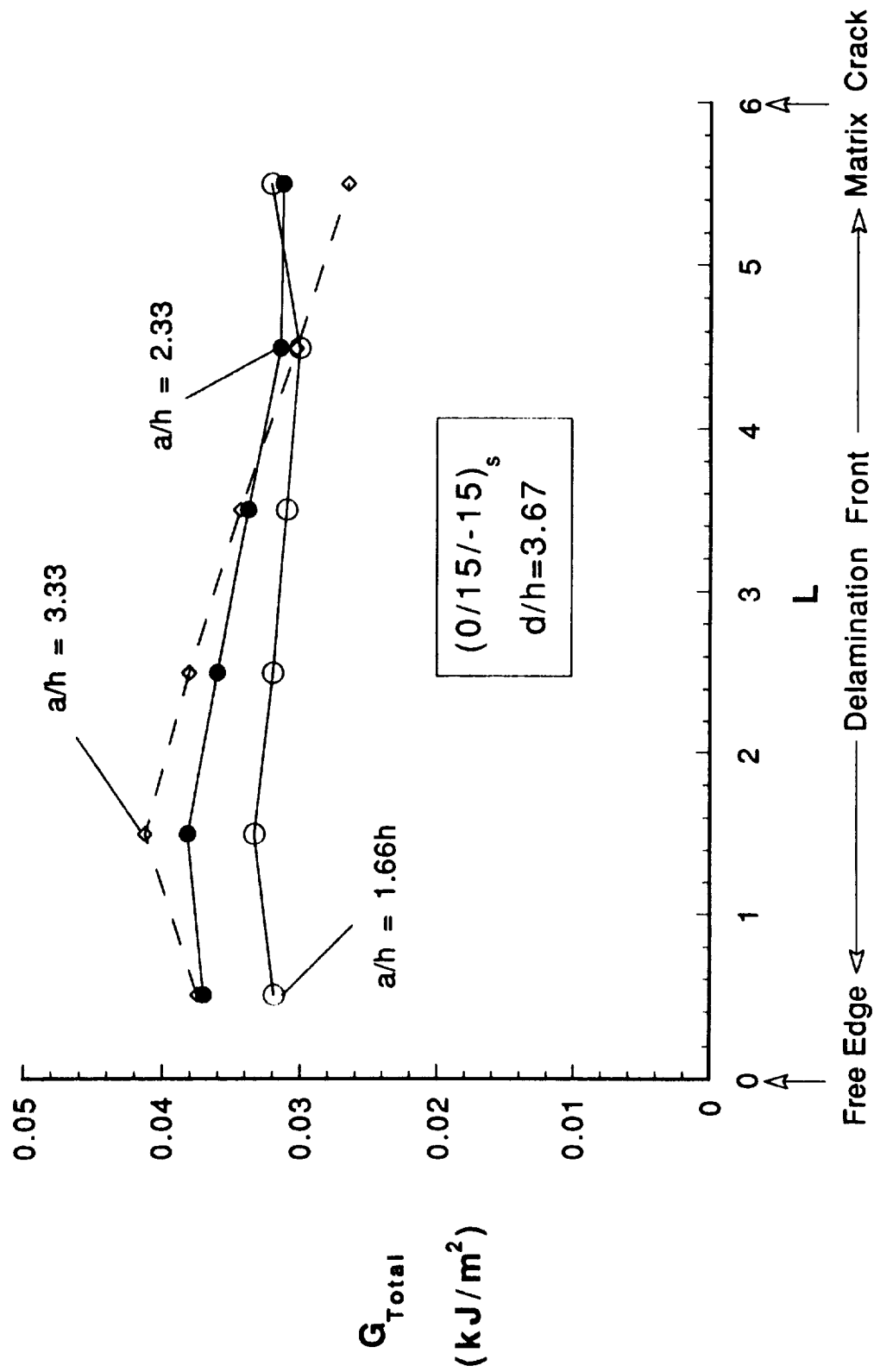


Fig.8 VCCT G Distribution Along Delamination Front in $(0/15/-15)_s$ laminate

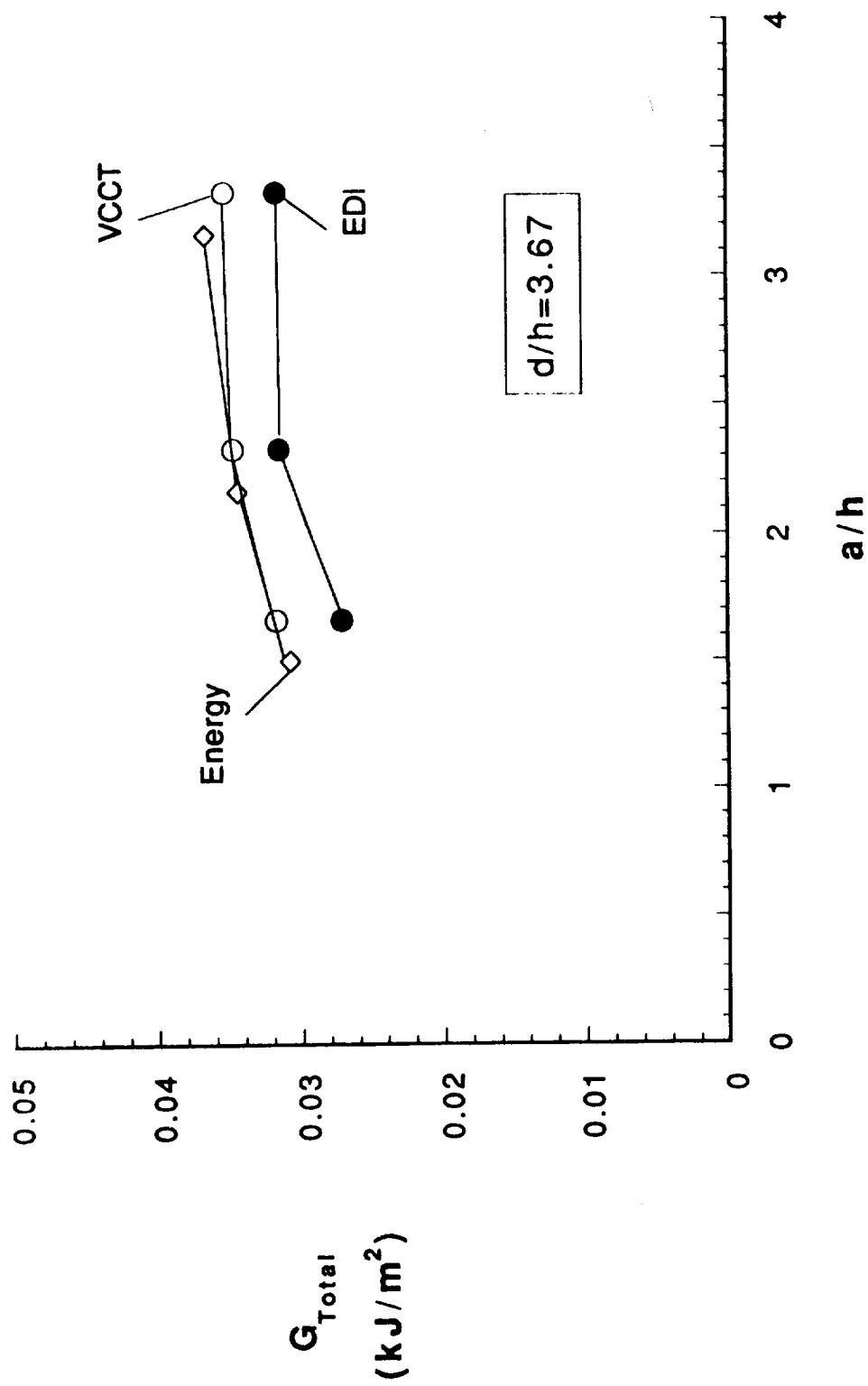


Fig.9 Average total Galong delamination front as a function of a/h for $(0/15/-15)_s$ laminate

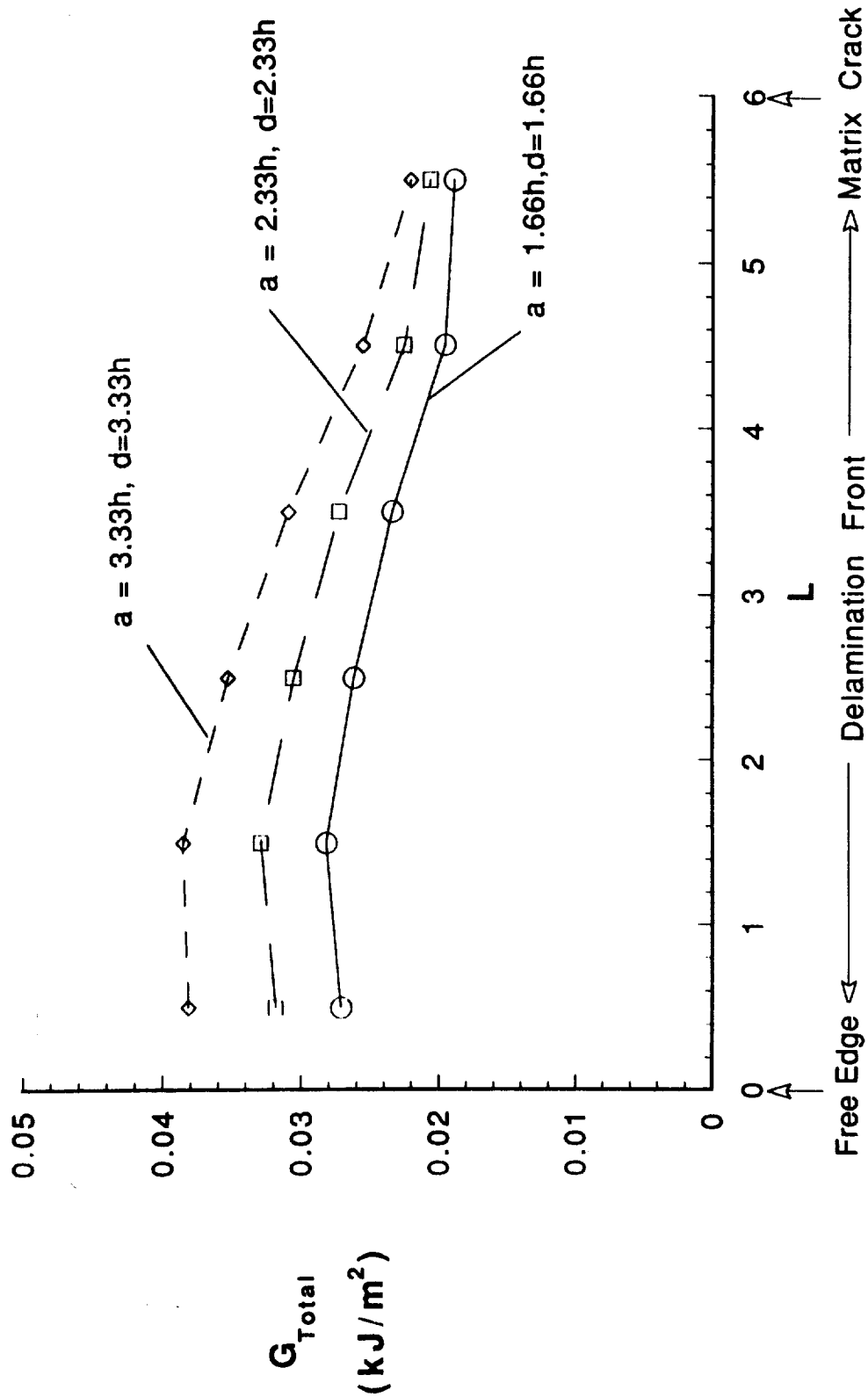


Fig.10 VCCT G Distribution Along Delamination Front in $(15/-15/0)_s$ laminate

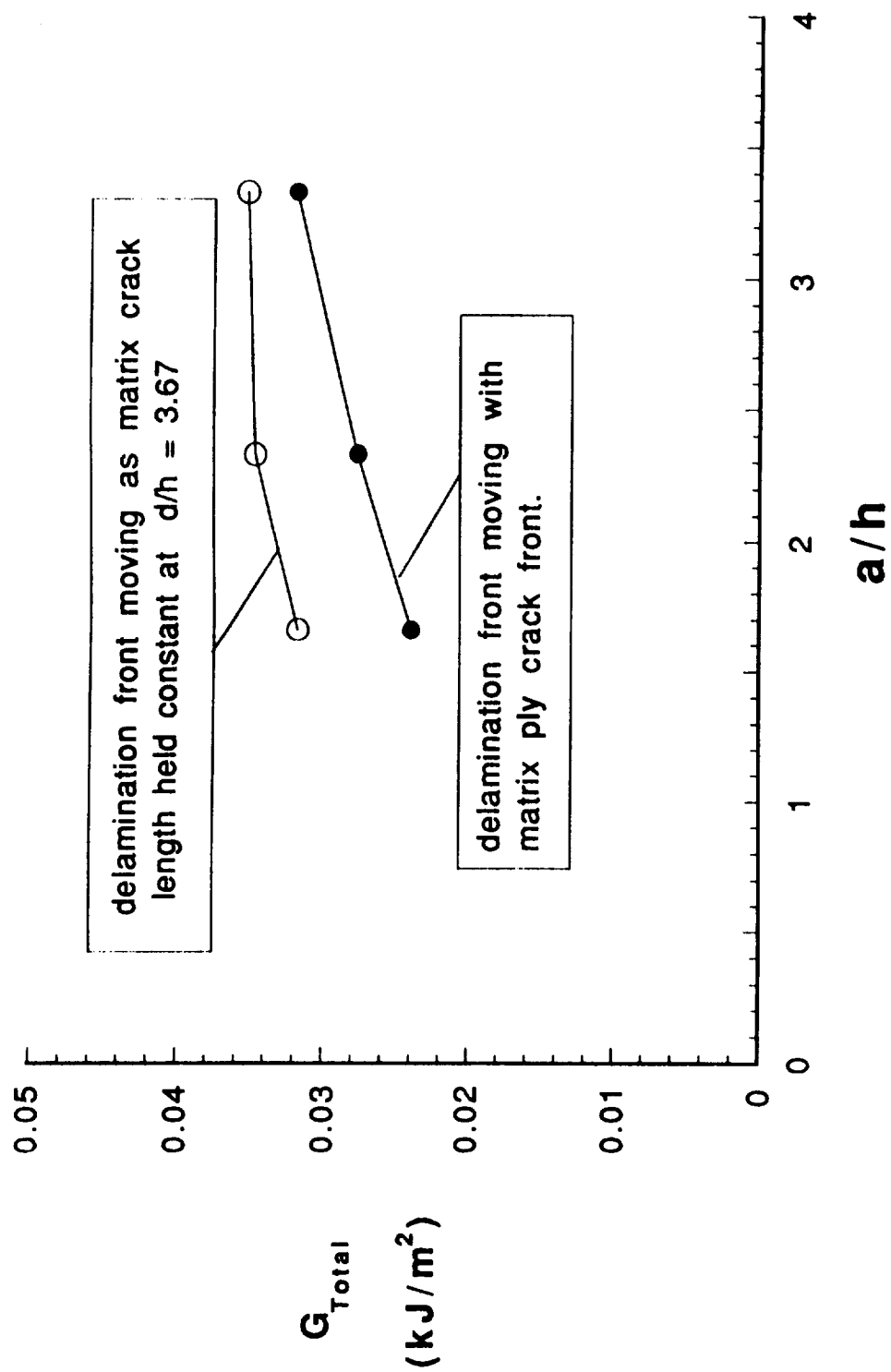


Fig.11 Average total G along delamination front as a function of a/h for $(0/15/-15)_s$ laminate

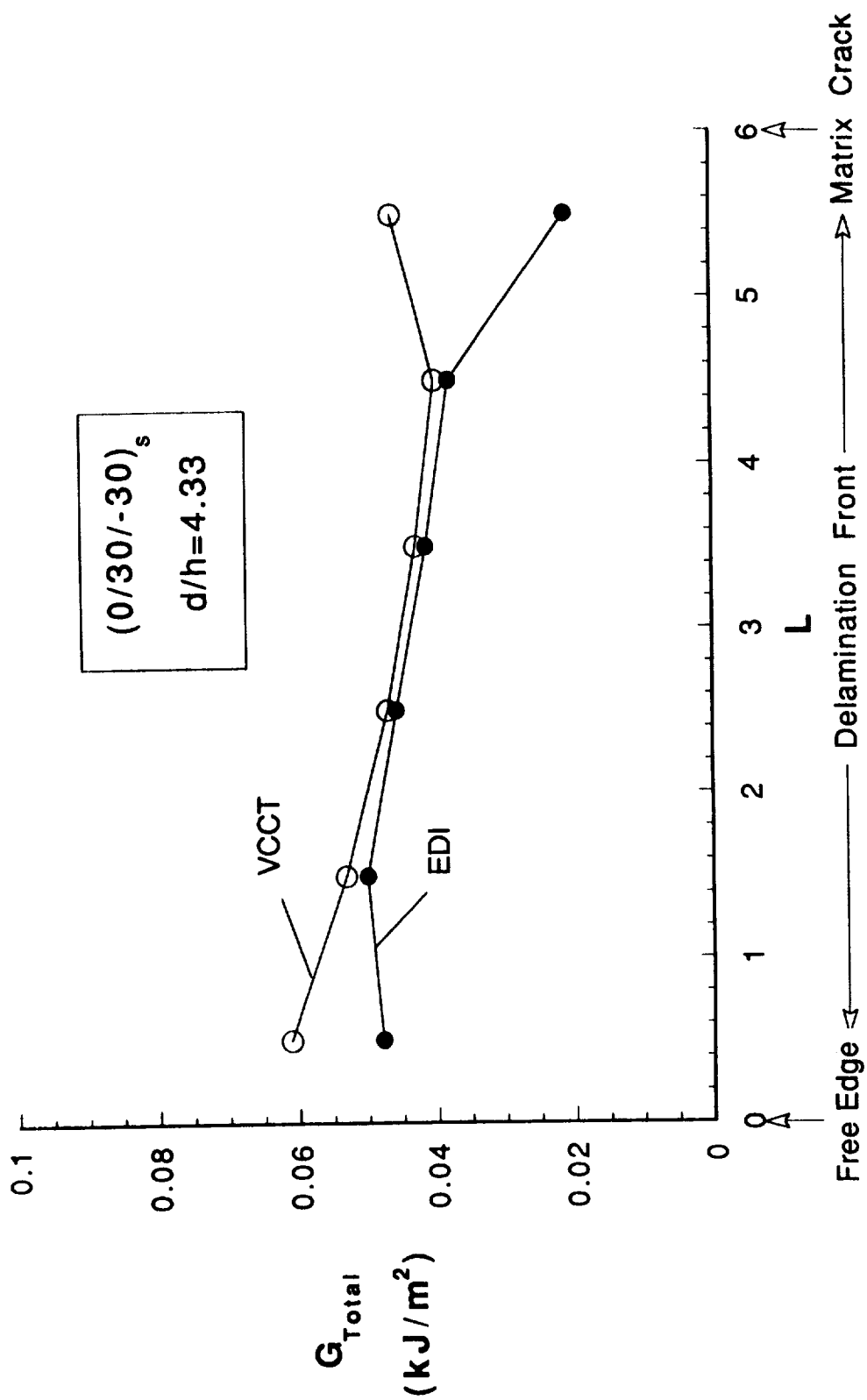


Fig.12 G Distribution Along Delamination Front in $(0/30/-30)_s$ laminate for $a/h=1.66$

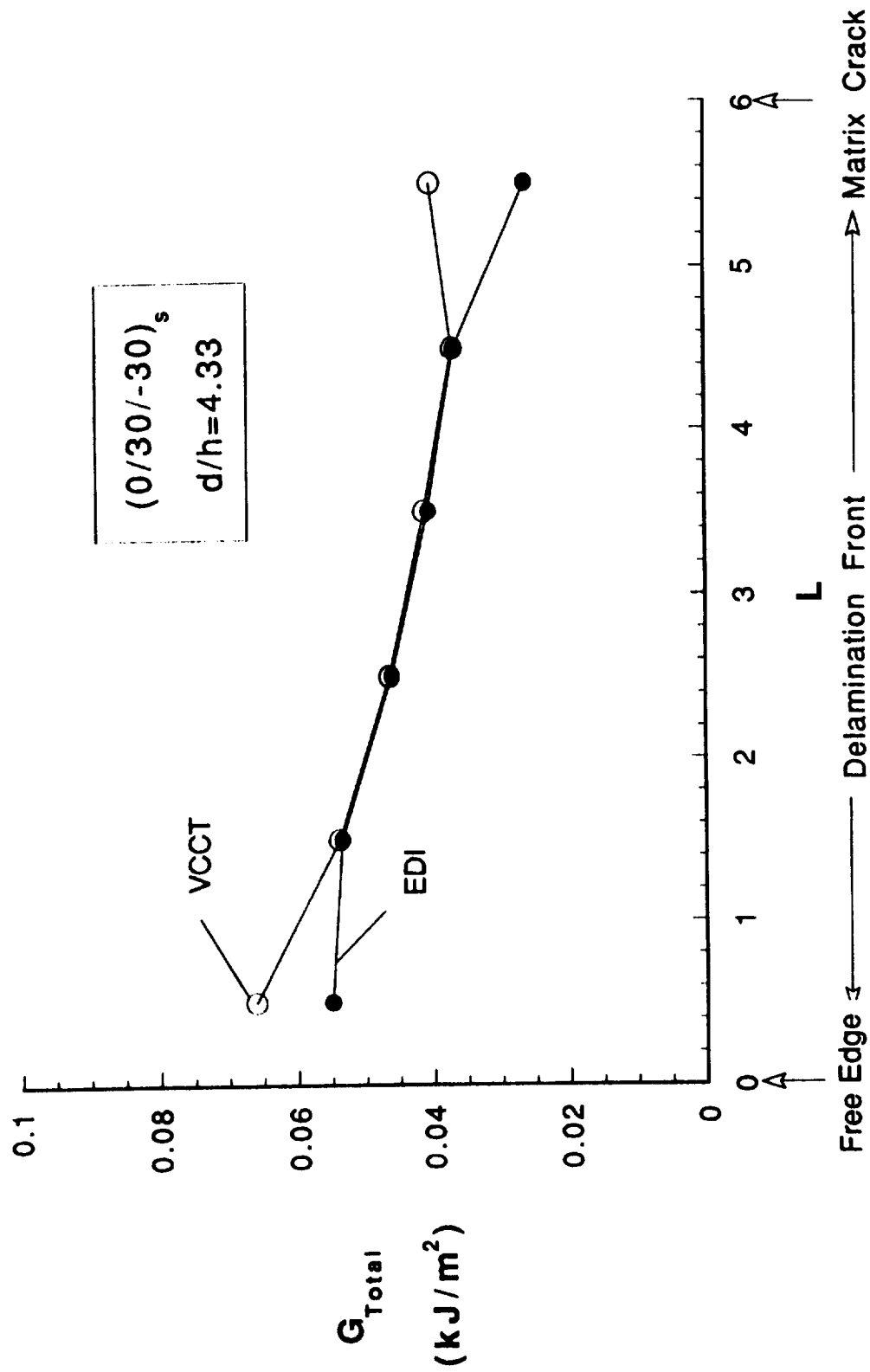


Fig.13 G Distribution Along Delamination Front in $(0/30/-30)_s$ laminate for $a/h=2.33$

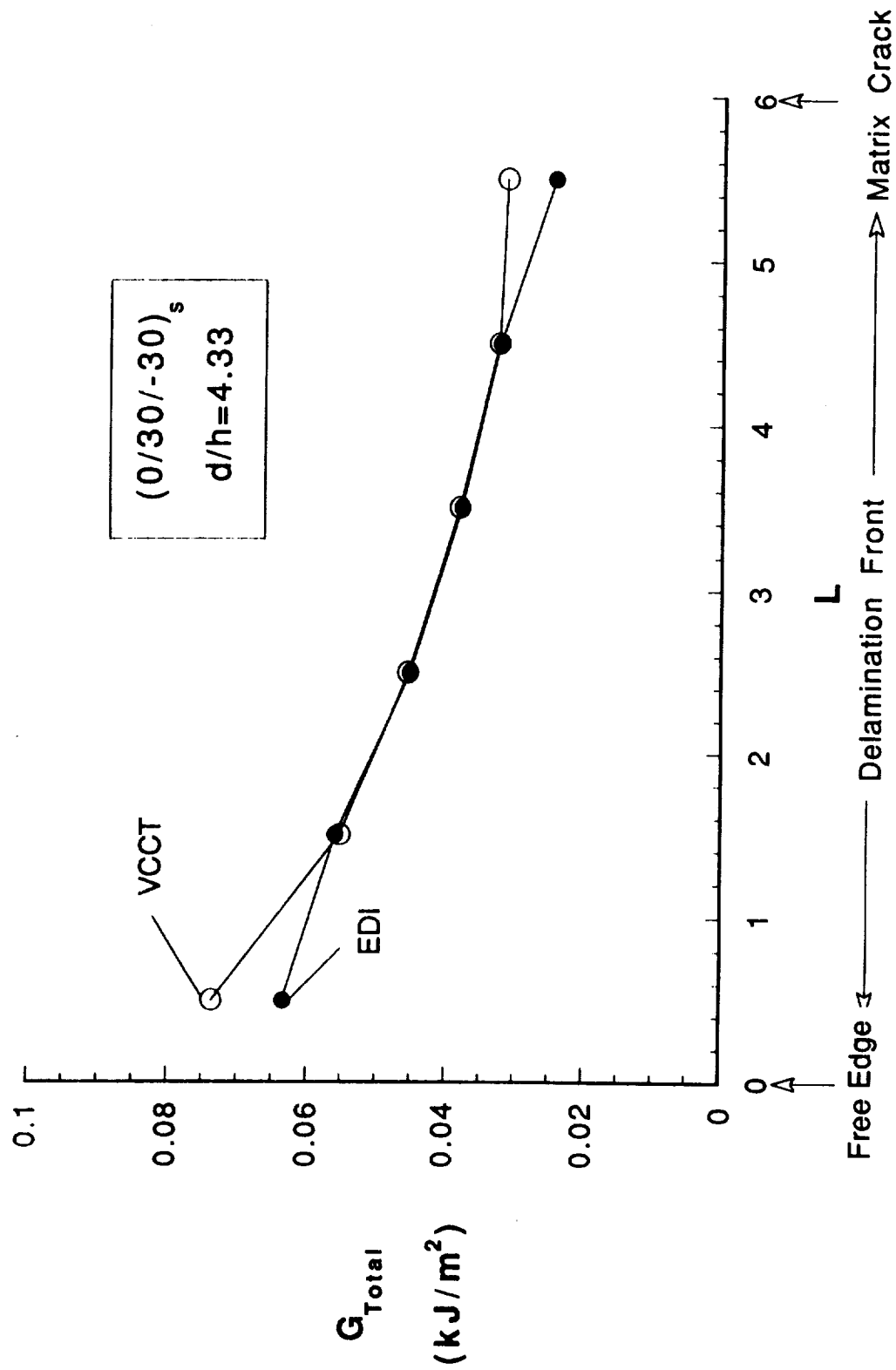


Fig.14 G Distribution Along Delamination Front in $(0/30/-30)_s$ laminate for $a/h=3.33$

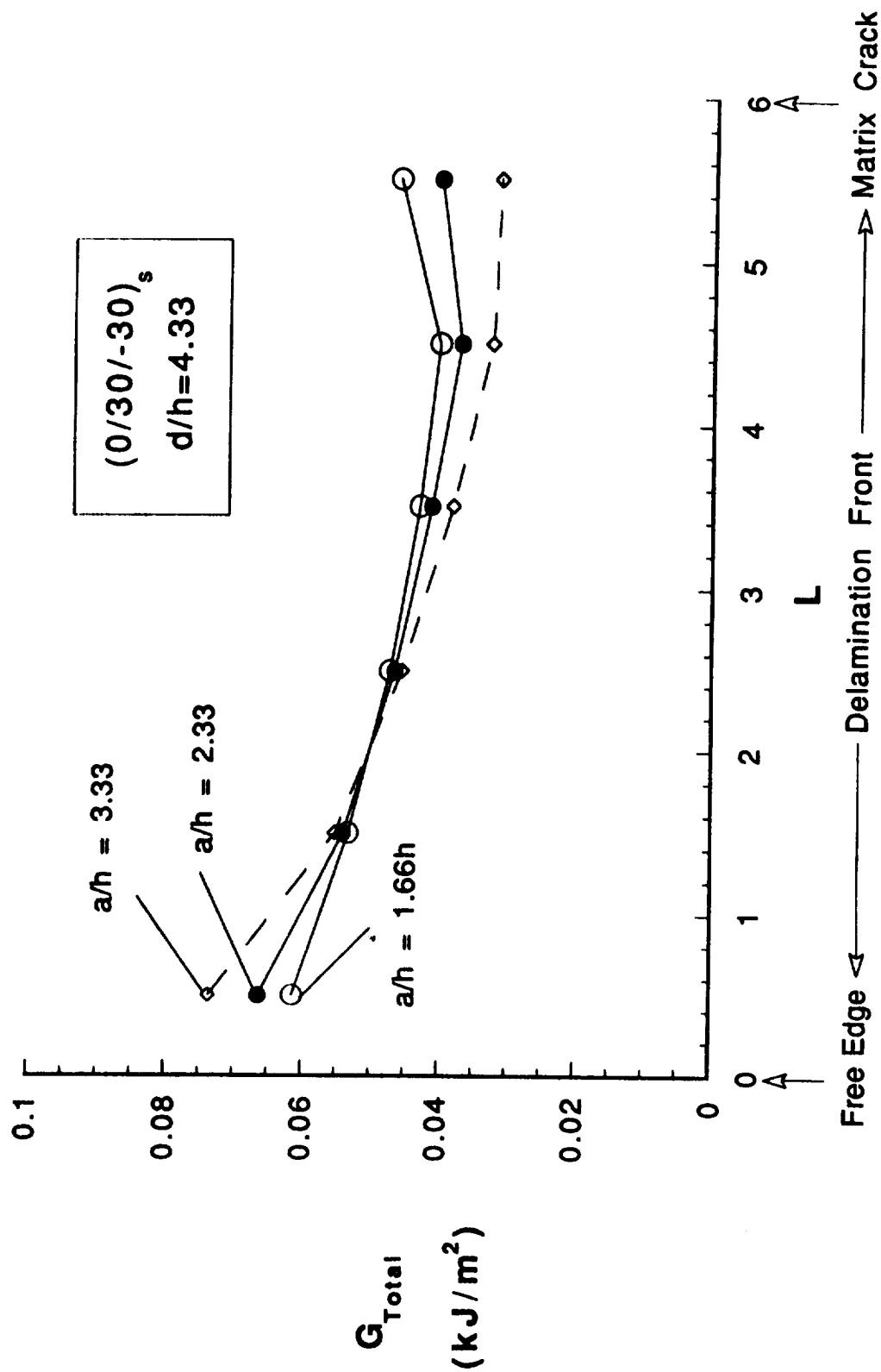


Fig.15 VCCT G Distribution Along Delamination Front in $(0/30/-30)_s$ laminate

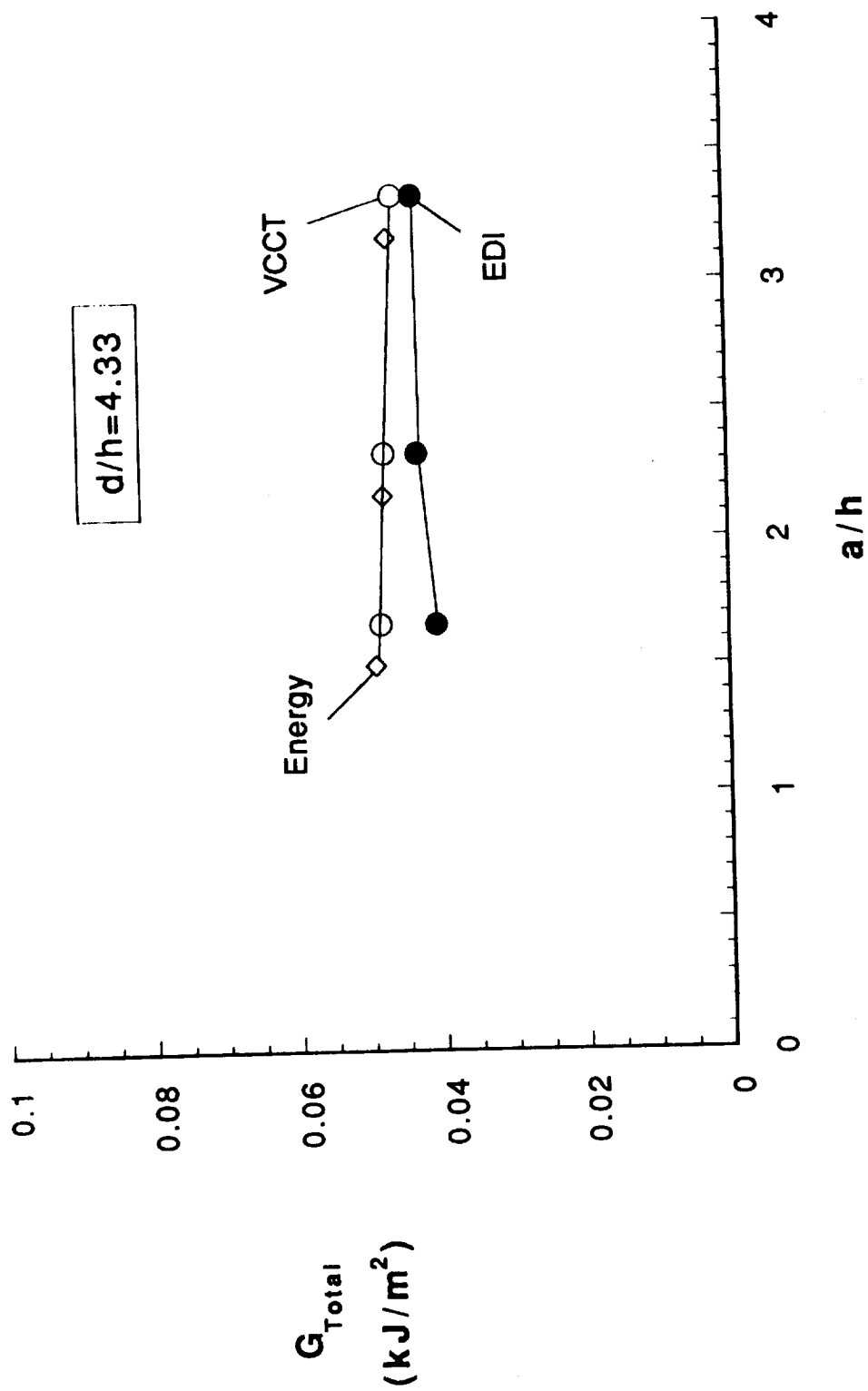


Fig.16 Average total Galong delamination front as a function of a/h for $(0/30/-30)_s$ laminate

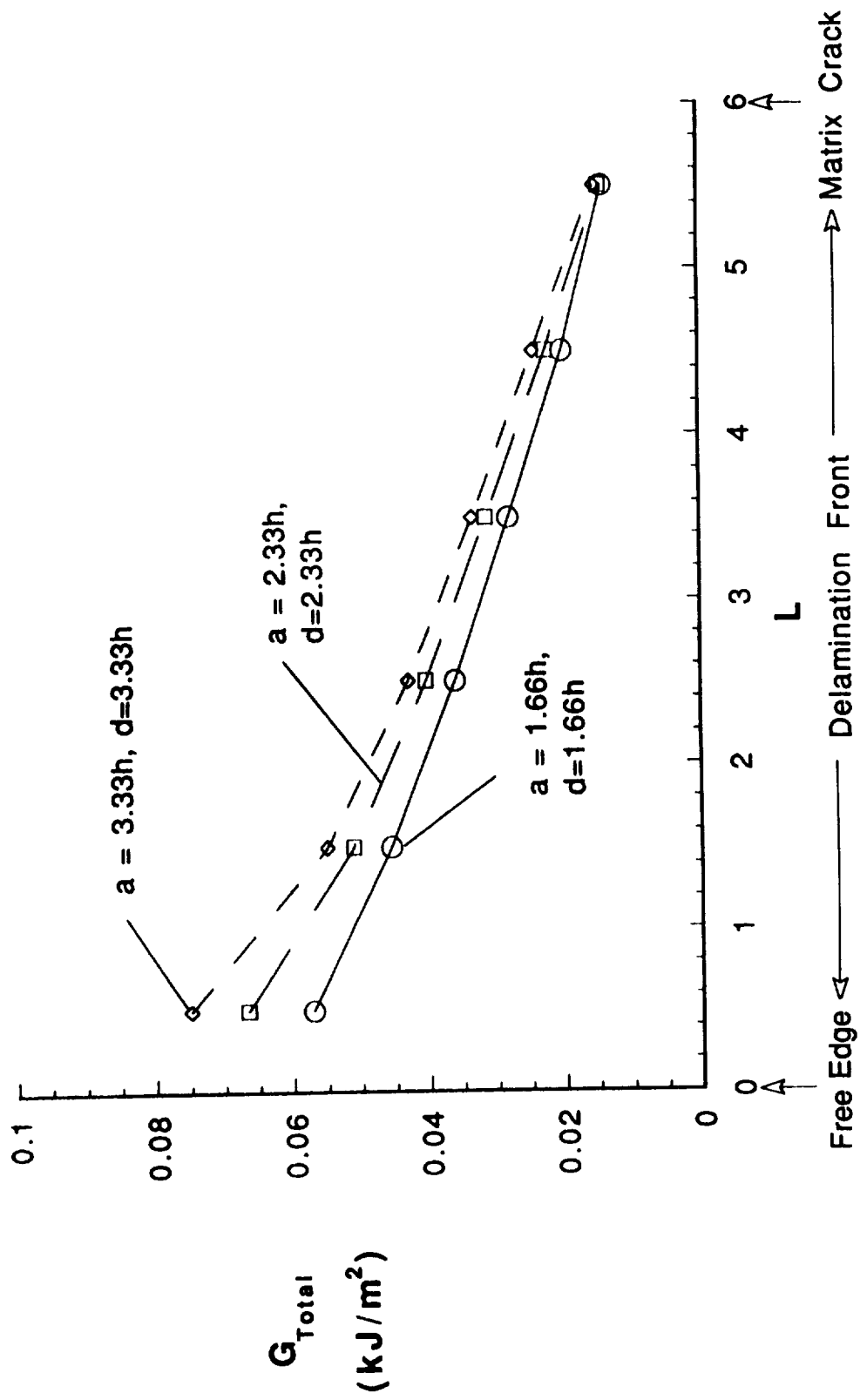


Fig.17 VCCT G Distribution Along Delamination Front in (0/30/-30)_s laminate

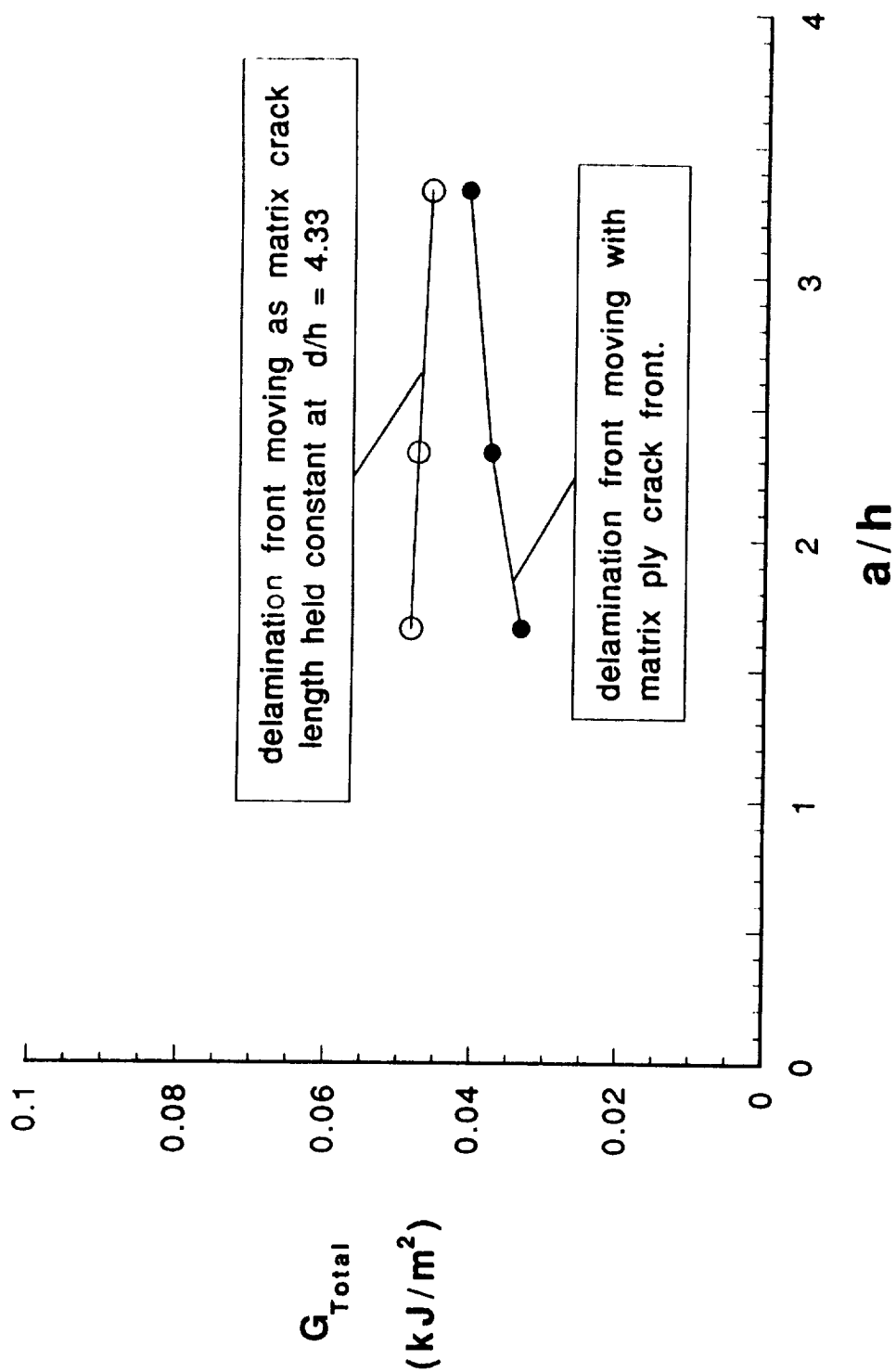


Fig.18 Average total Galong delamination front as a function of a/h for $(0/30/-30)_s$ laminate

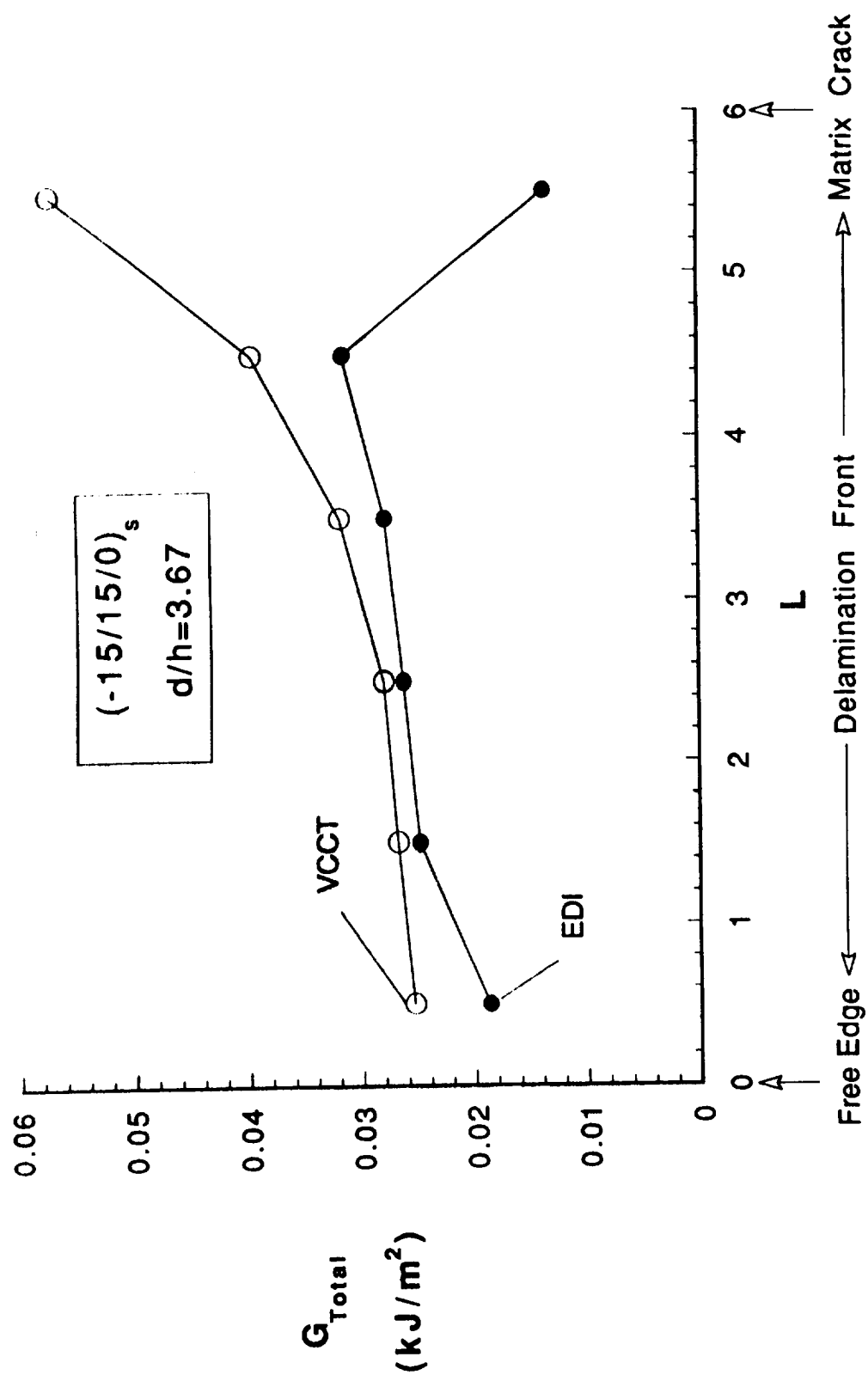


Fig.19 G Distribution Along Delamination Front in $(-15/15/0)_s$ laminate for $a/h=1.66$

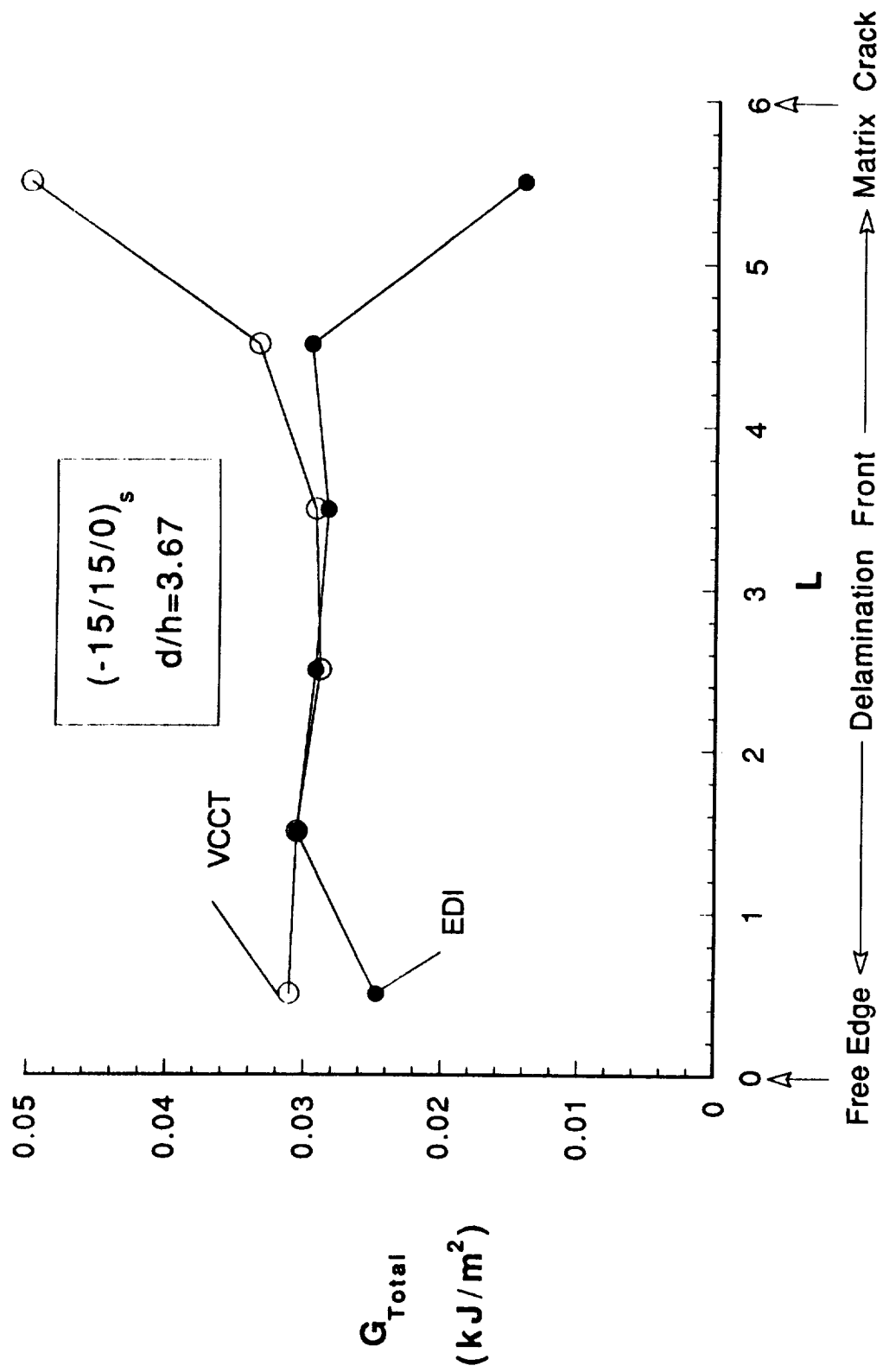


Fig.20 G Distribution Along Delamination Front in $(-15/15/0)_s$ laminate for $a/h=2.33$

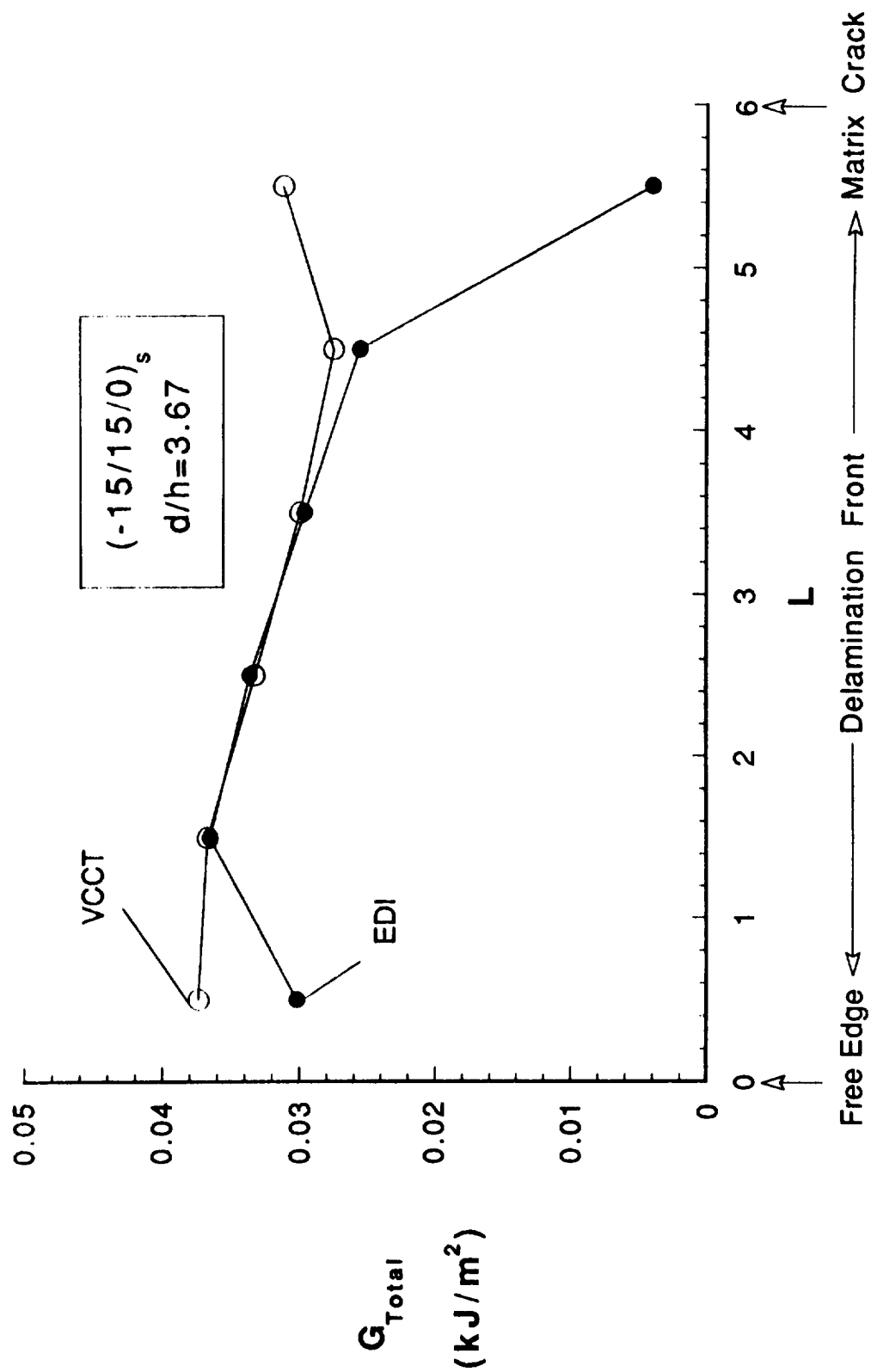


Fig.21 G Distribution Along Delamination Front in $(-15/15/0)_s$ laminate for $a/h=3.33$

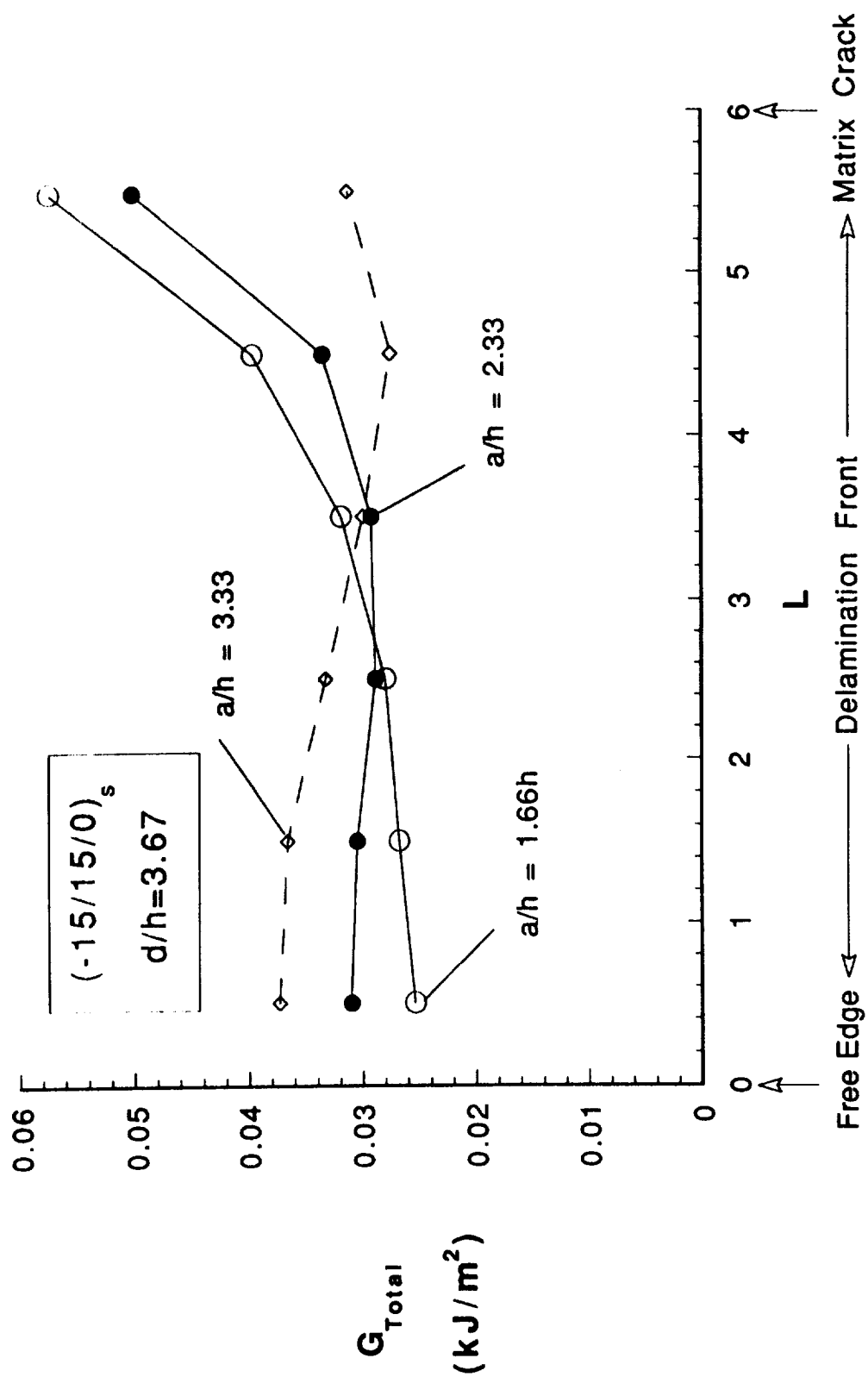


Fig.22 VCCT G Distribution Along Delamination Front in $(-15/15/0)_s$ laminate

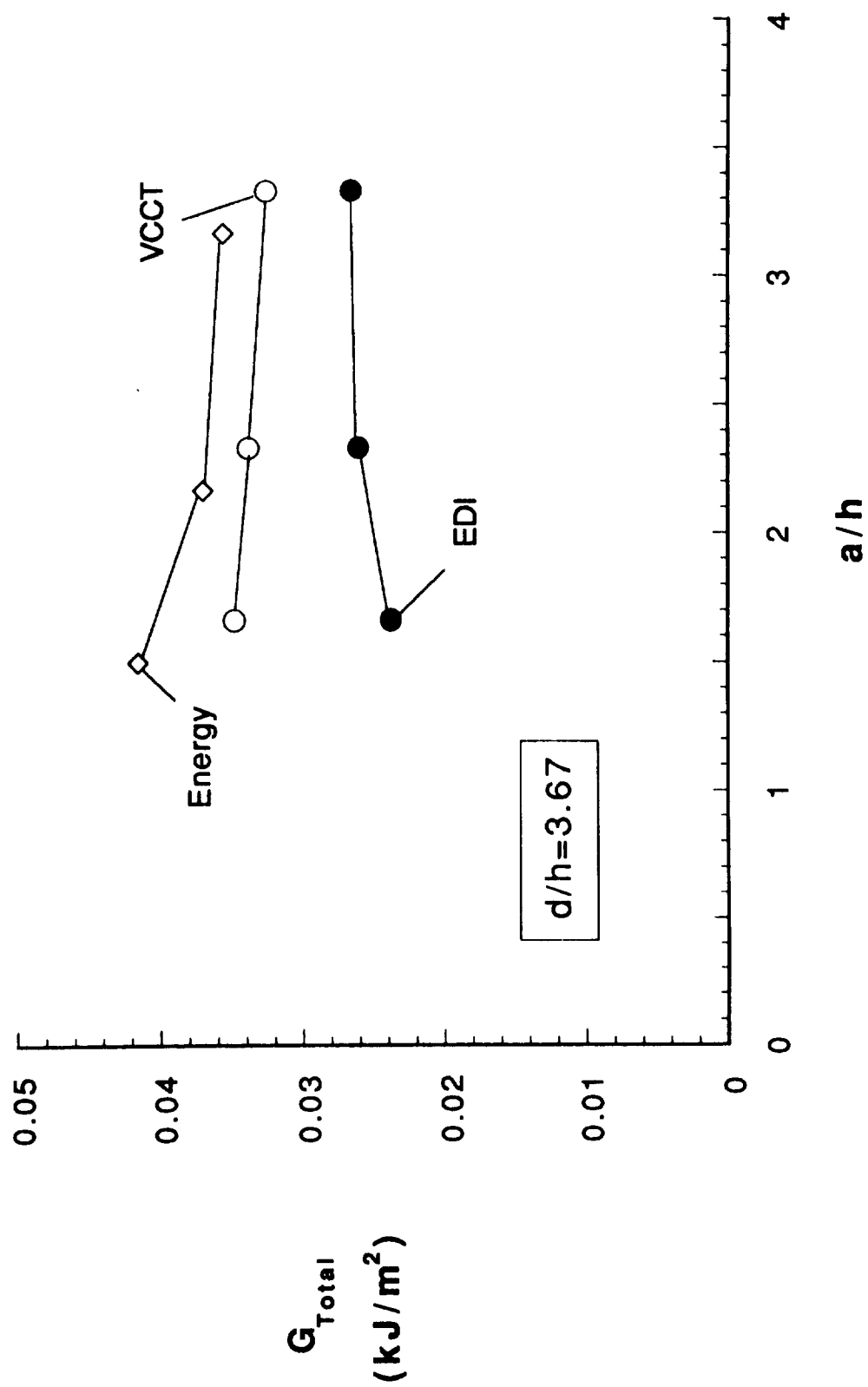


Fig.23 Average total Galong delamination front as a function of a/h for $(-15/15/0)_s$ laminate

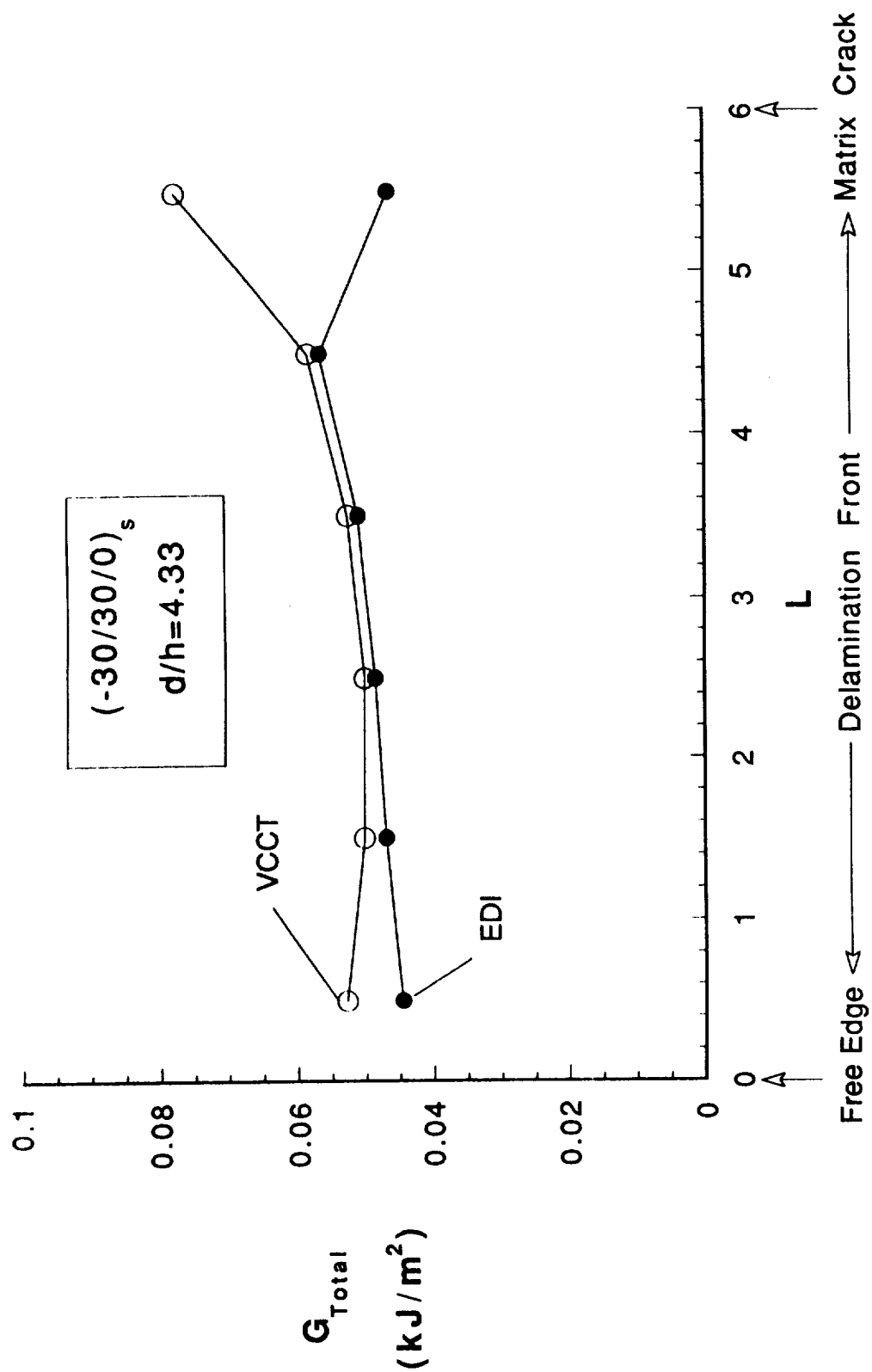


Fig.24 G Distribution Along Delamination Front in $(-30/30/0)_s$ laminate for $a/h=1.66$

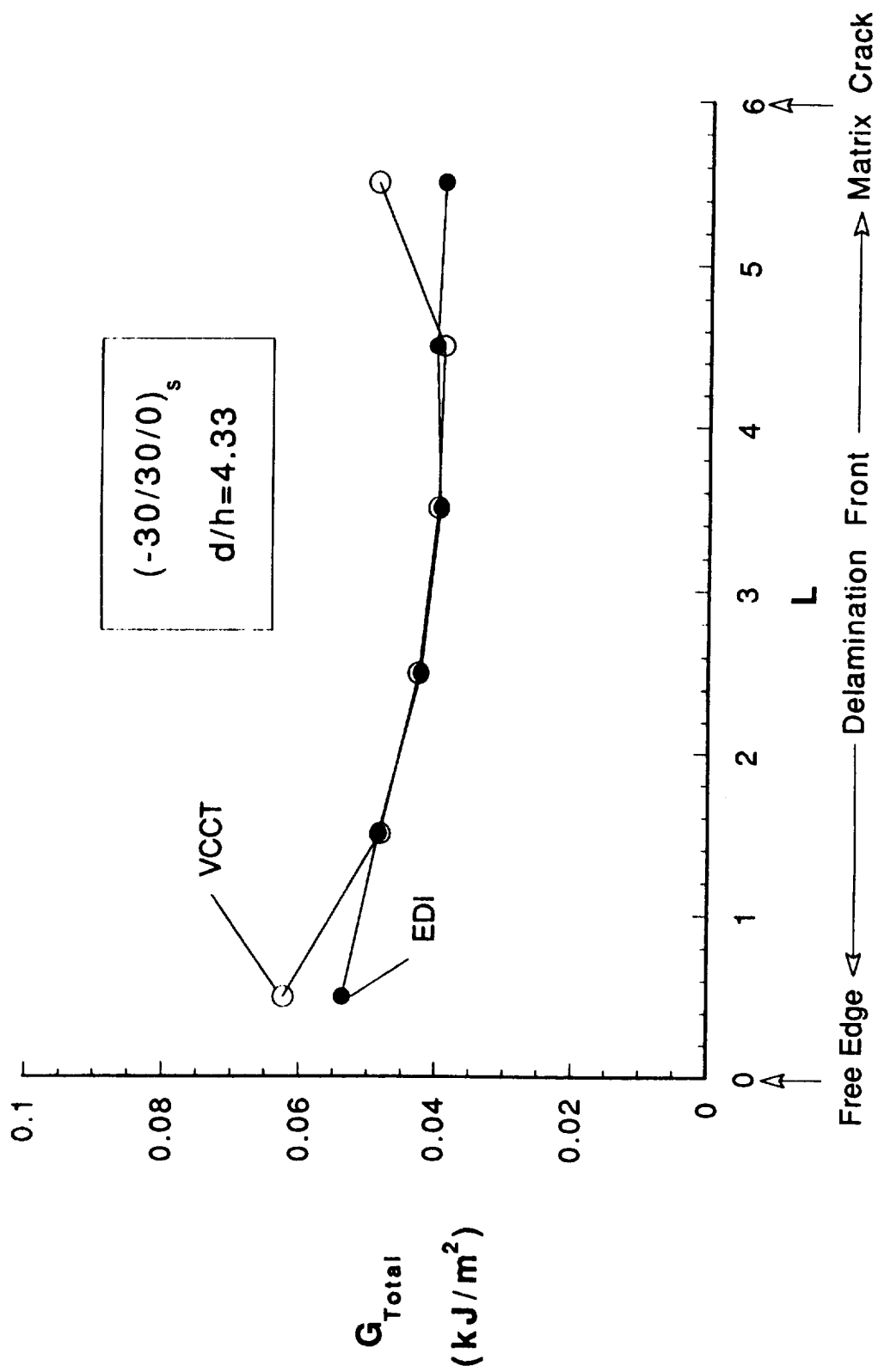


Fig.25 G Distribution Along Delamination Front in $(-30/30/0)_s$ laminate for $a/h=3.33$

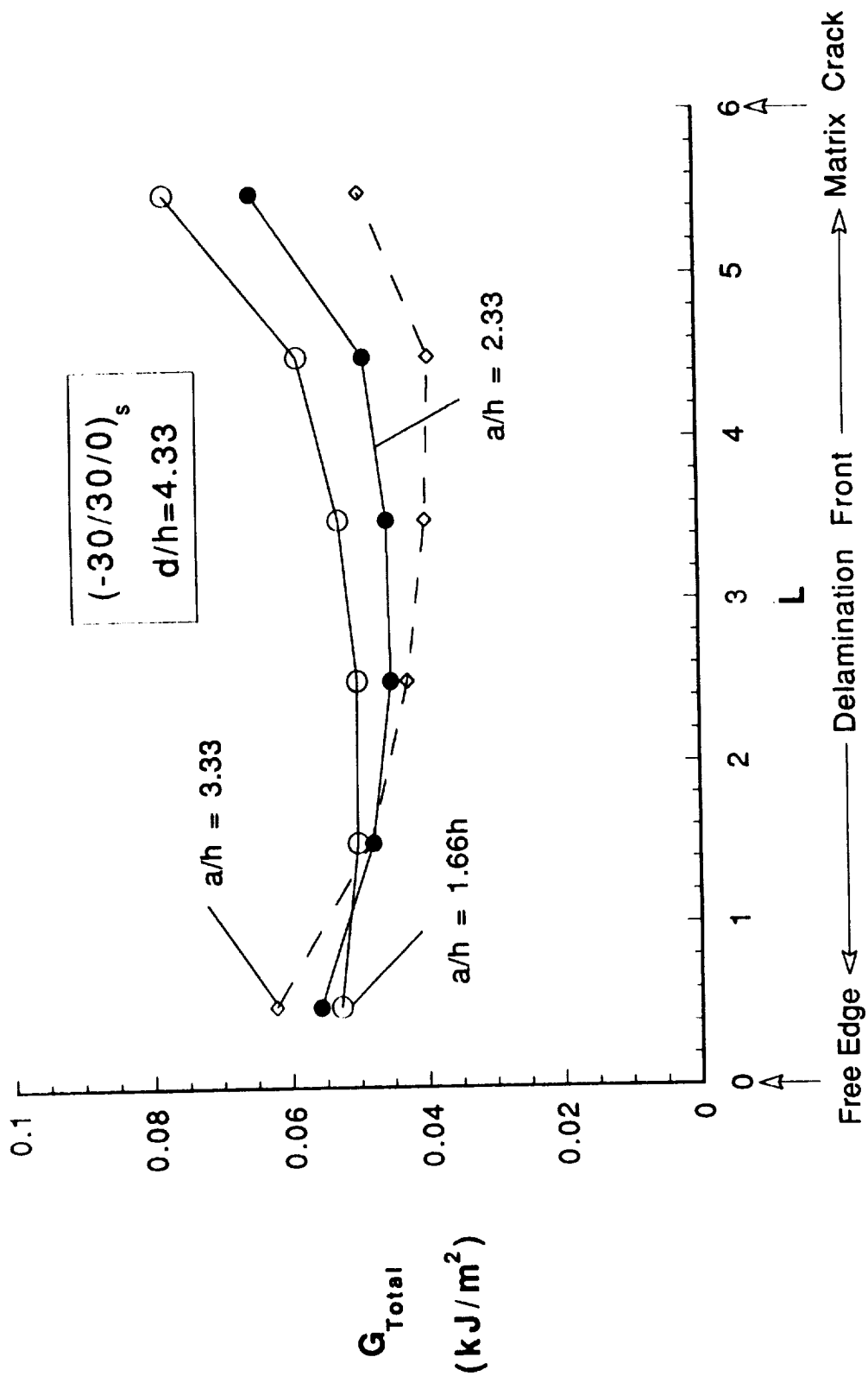


Fig.26 VCCT G Distribution Along Delamination Front in $(-30/30/0)_s$ laminate

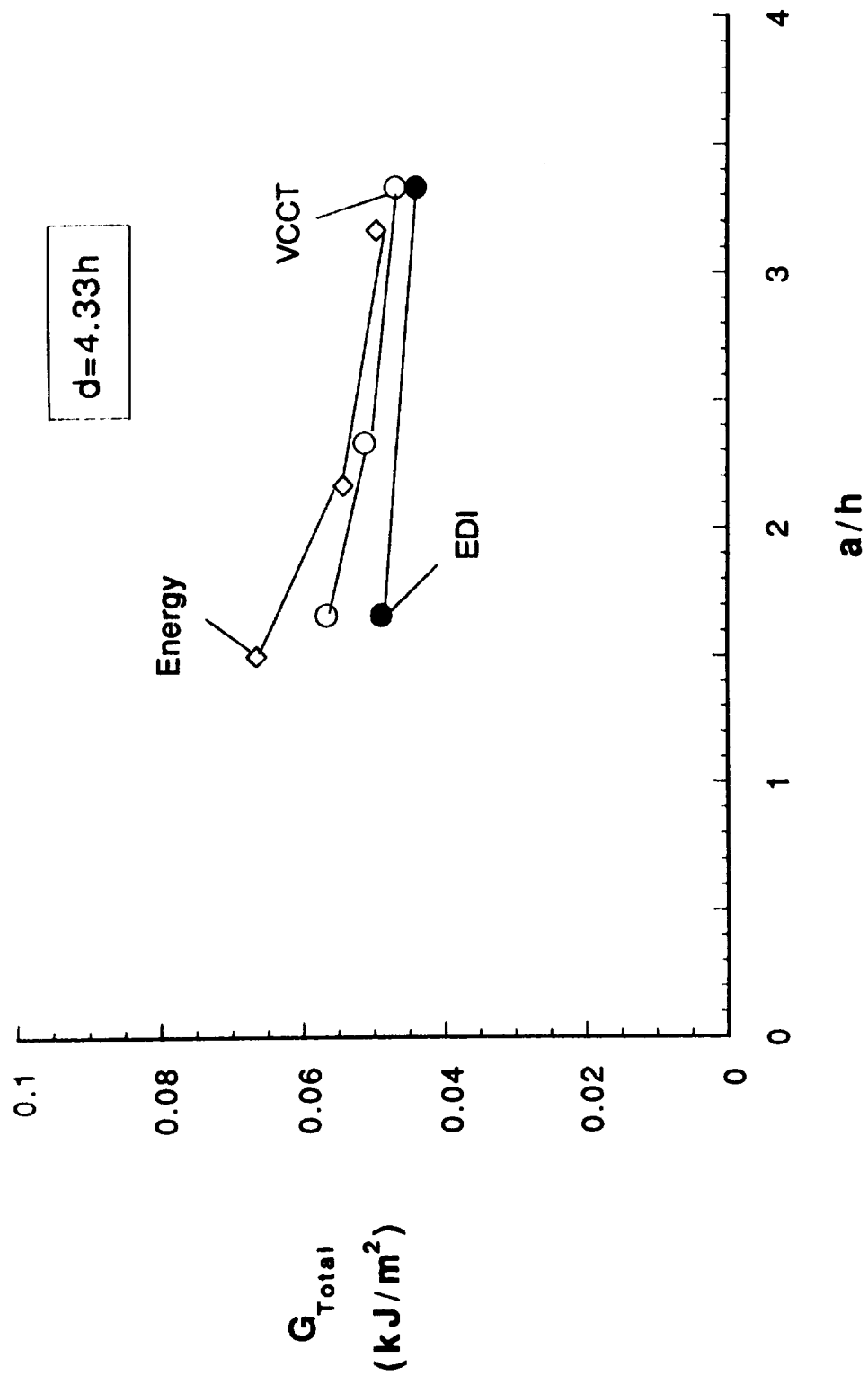


Fig.27 Average total Galong delamination front as a function of a/h for $(-30/30/0)_s$ laminate

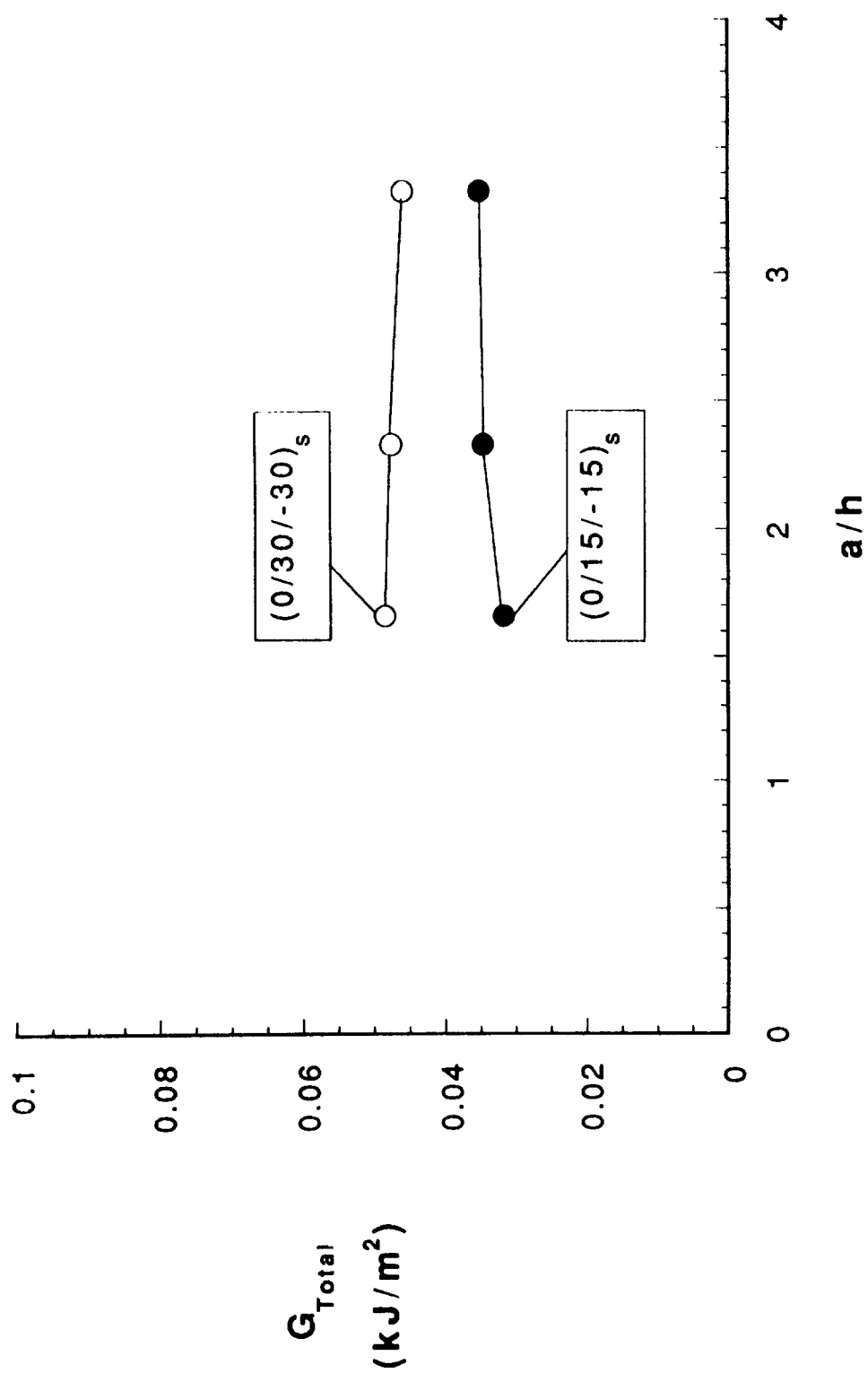


Fig.28 Comparison of average VCCT total G along delamination front as a function of a/h

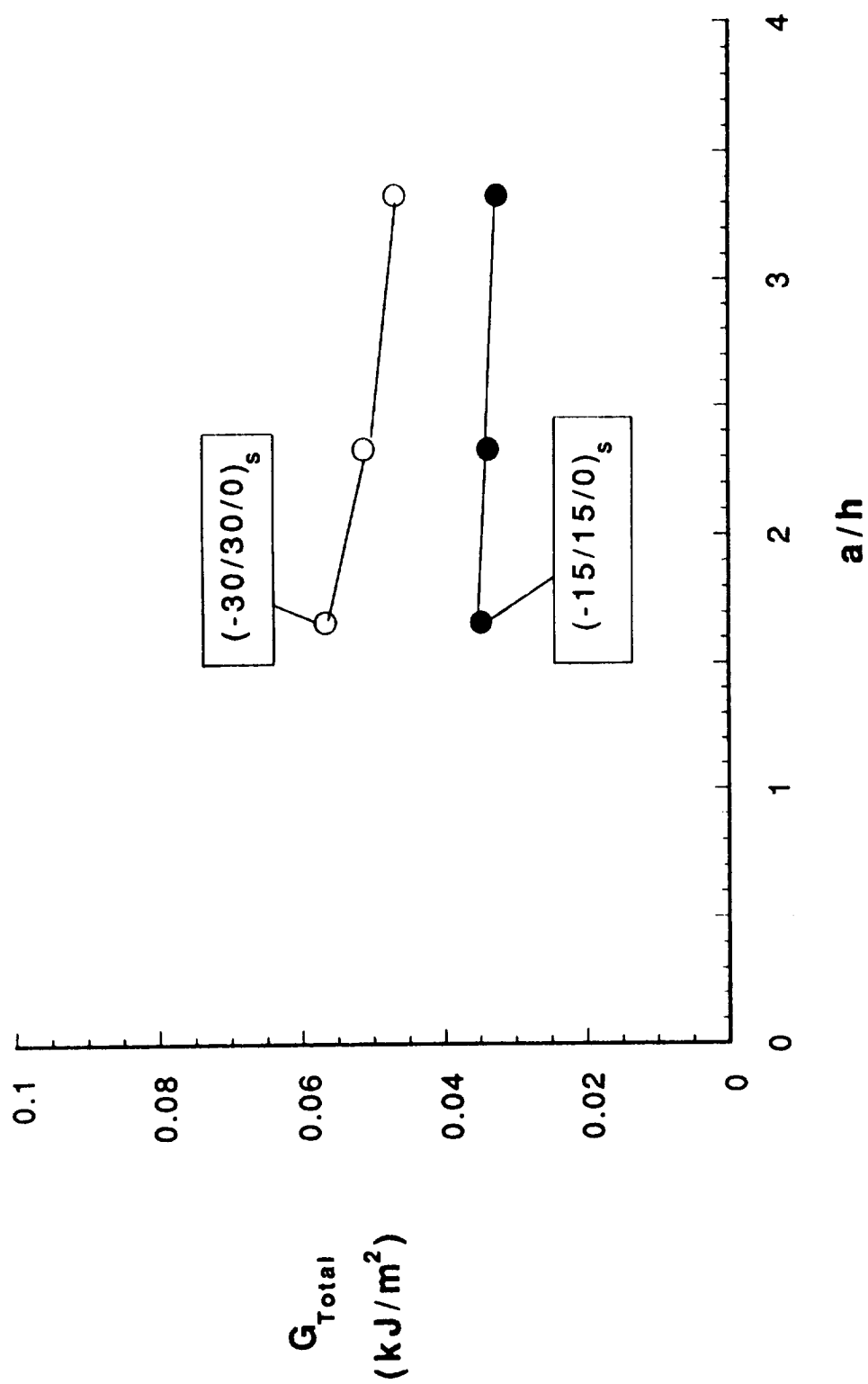


Fig.29 Comparison of average VCCT total G along delamination front as a function of a/h

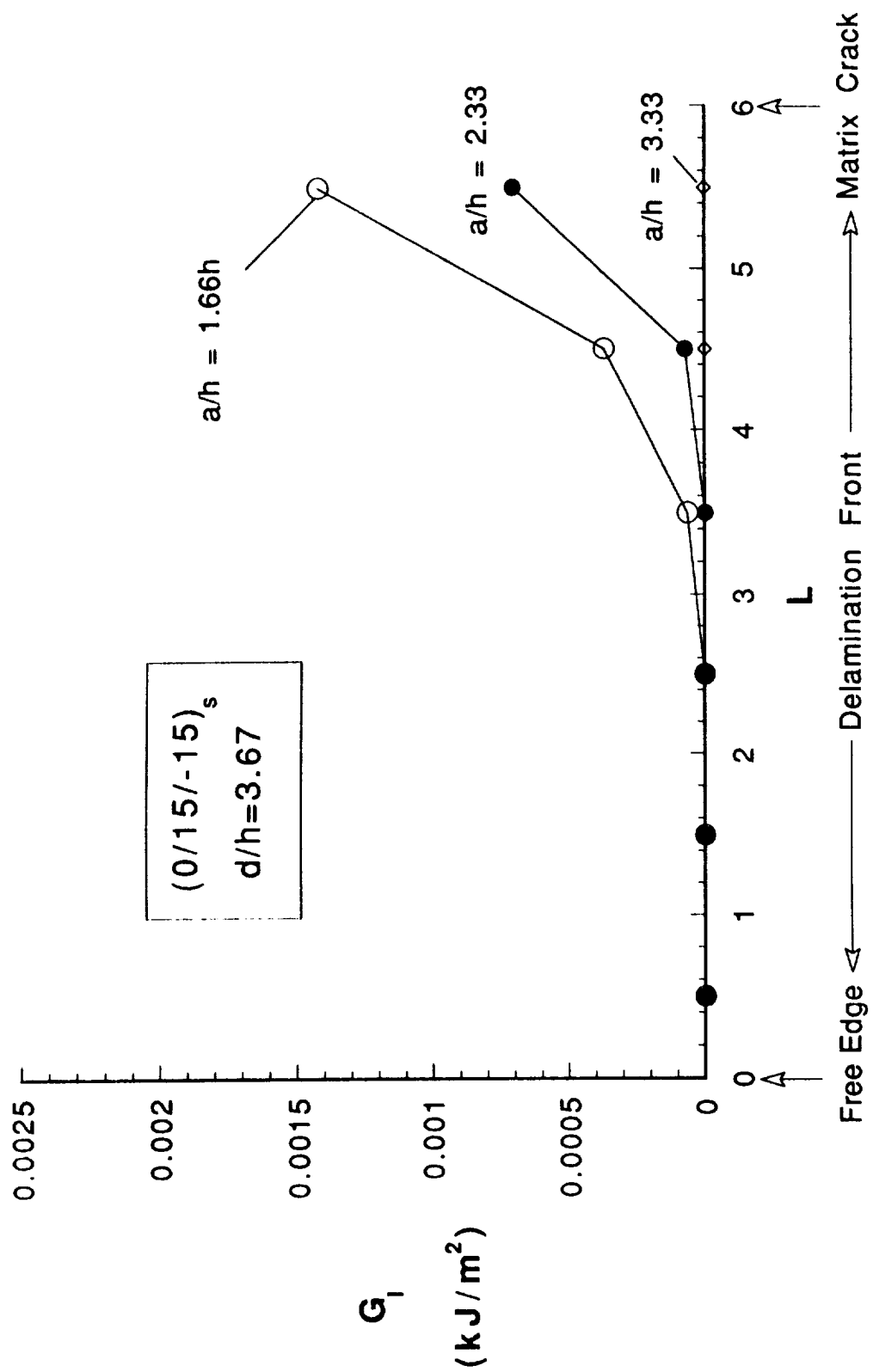


Fig.30 VCCT G_I distribution along delamination front in $(0/15/-15)_s$ laminate

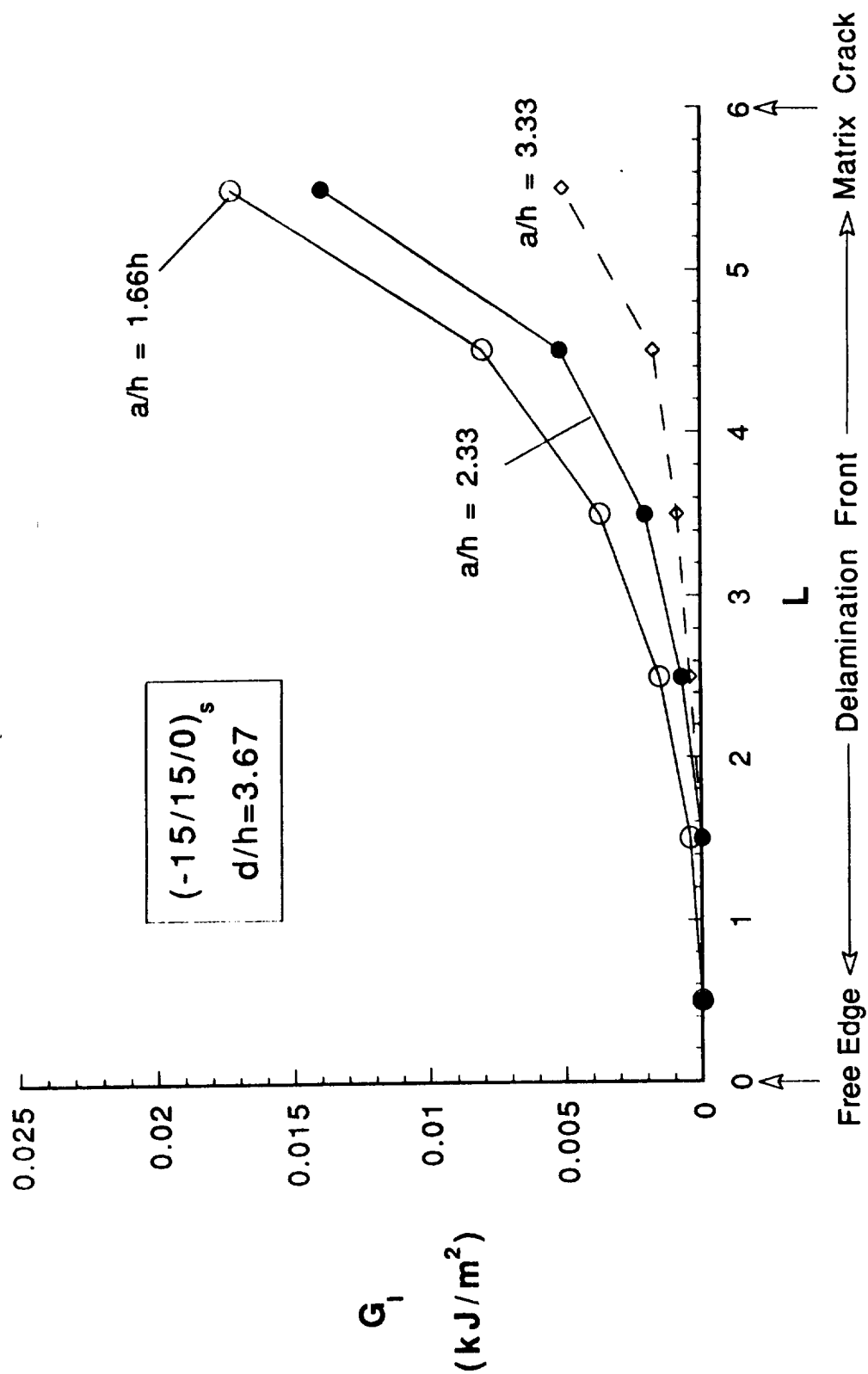


Fig.31 VCCT G_I distribution along delamination front in $(-15/15/0)_s$ laminate

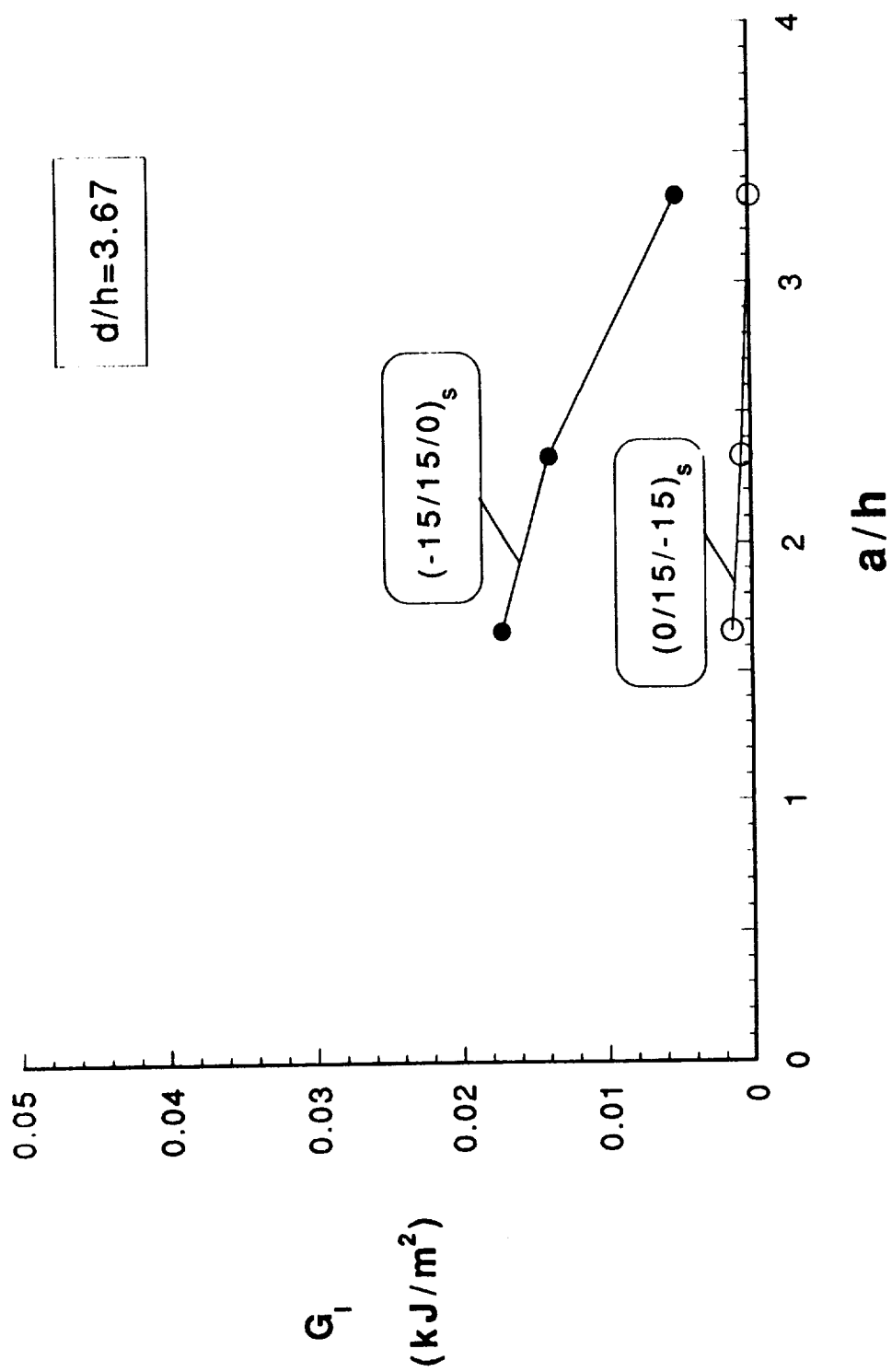


Fig.32 G_I near matrix crack as a function of a/h

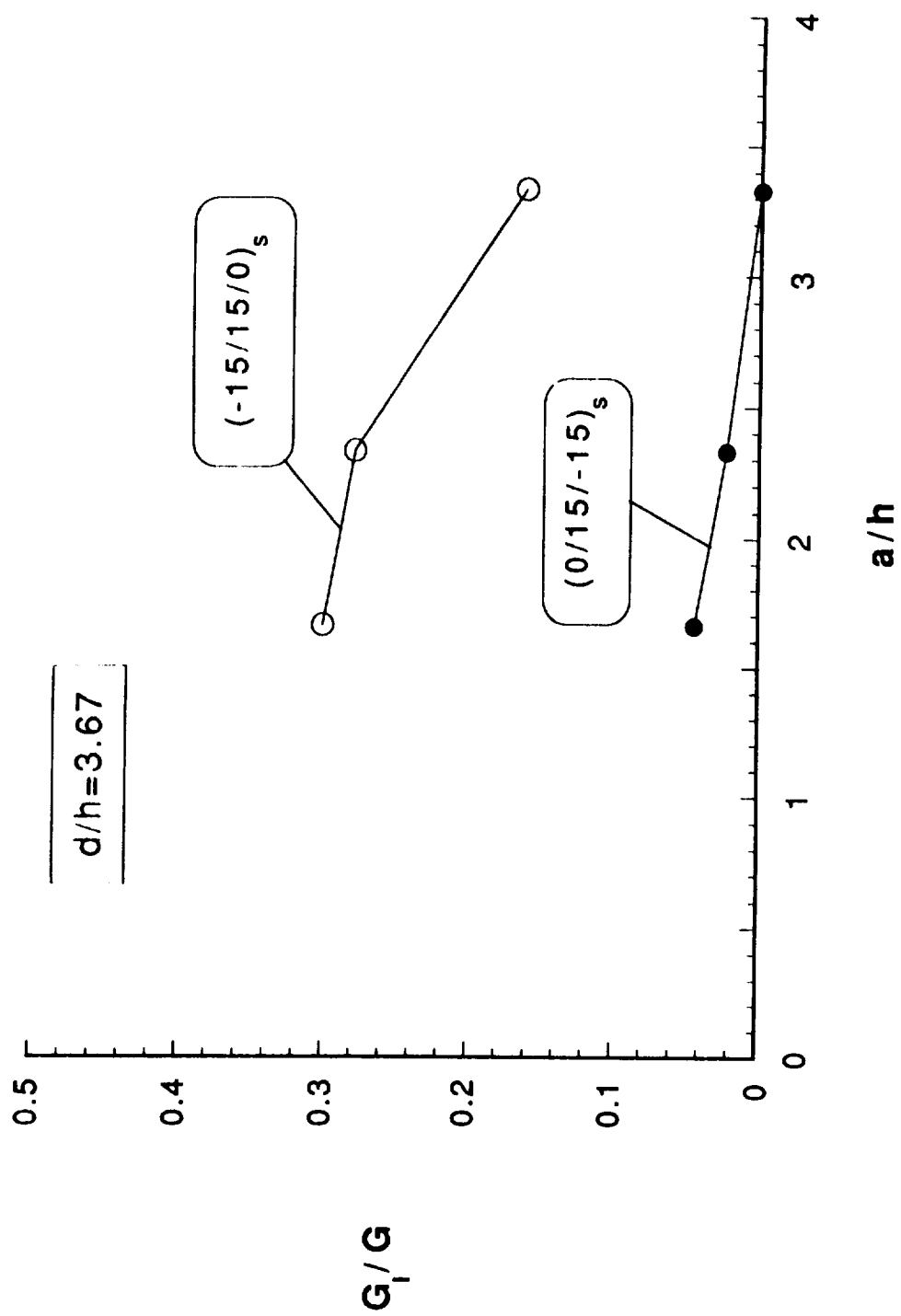


Fig.33 G_I/G near matrix crack front as a function of a/h

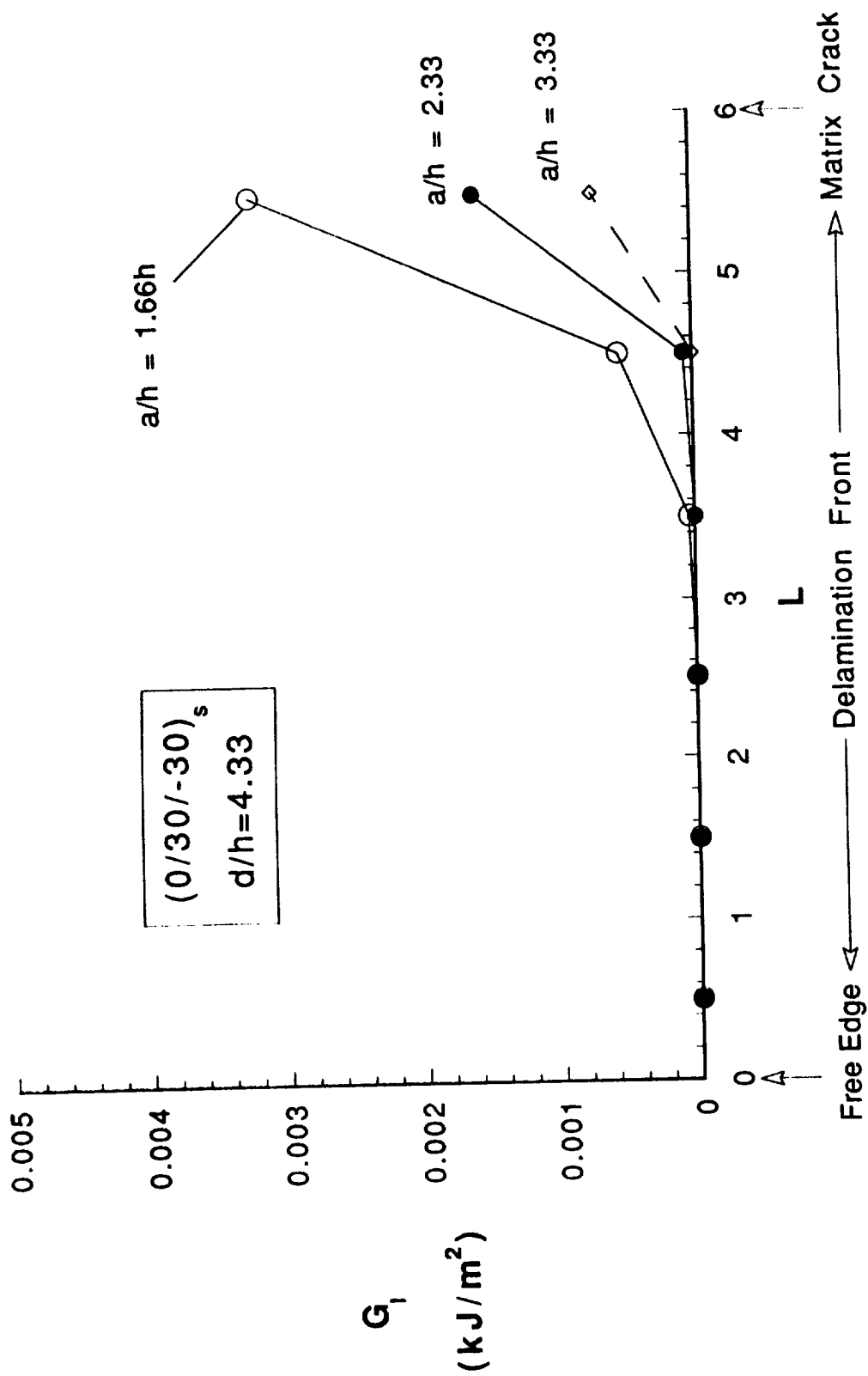


Fig.34 VCCT G_I distribution along delamination front in $(0/30/-30)_s$ laminate

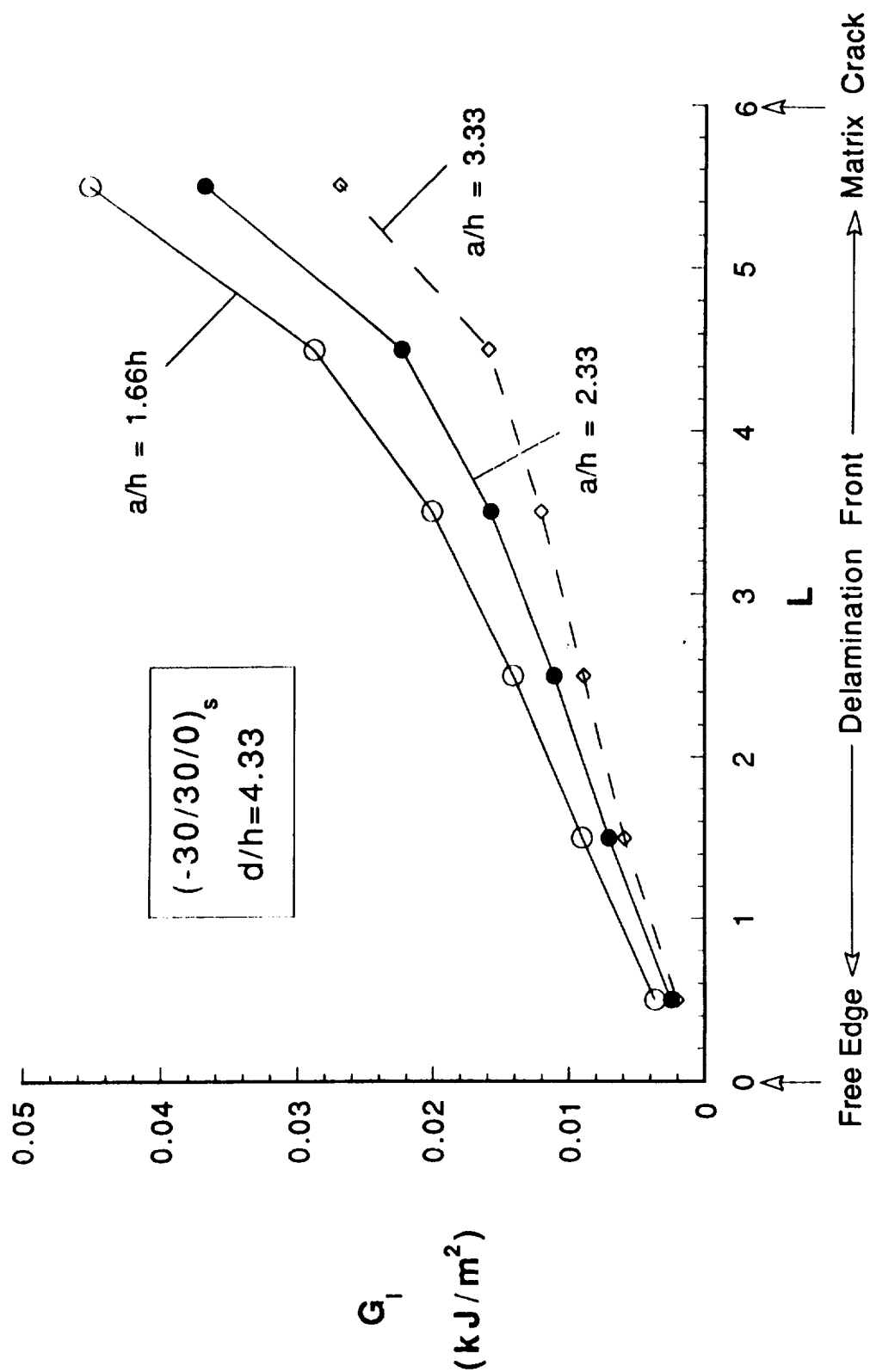


Fig.35 VCCT G_I distribution along delamination front in $(-30/30/0)_s$ laminate

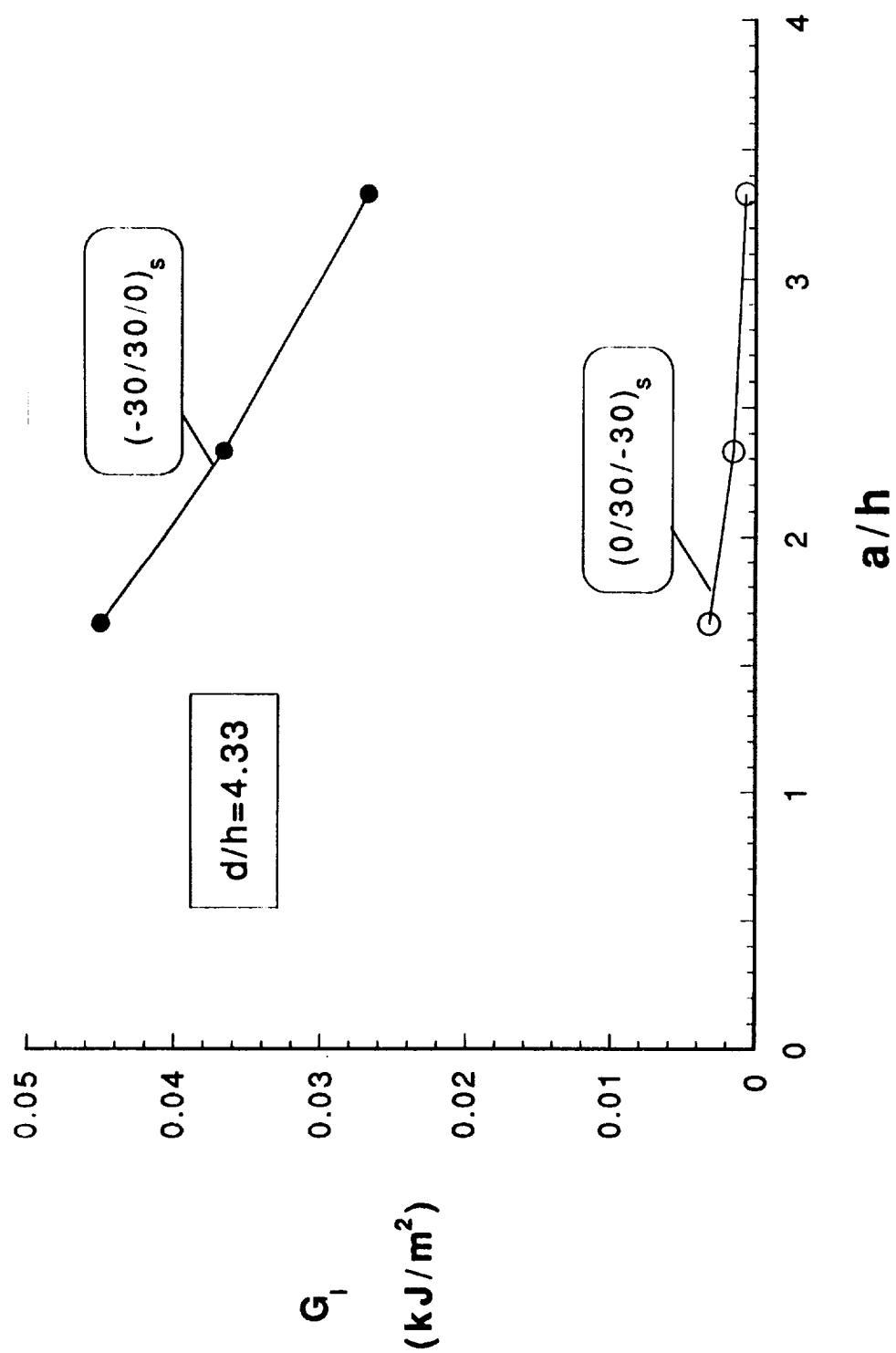


Fig.36 G_I near matrix crack front as a function of a/h

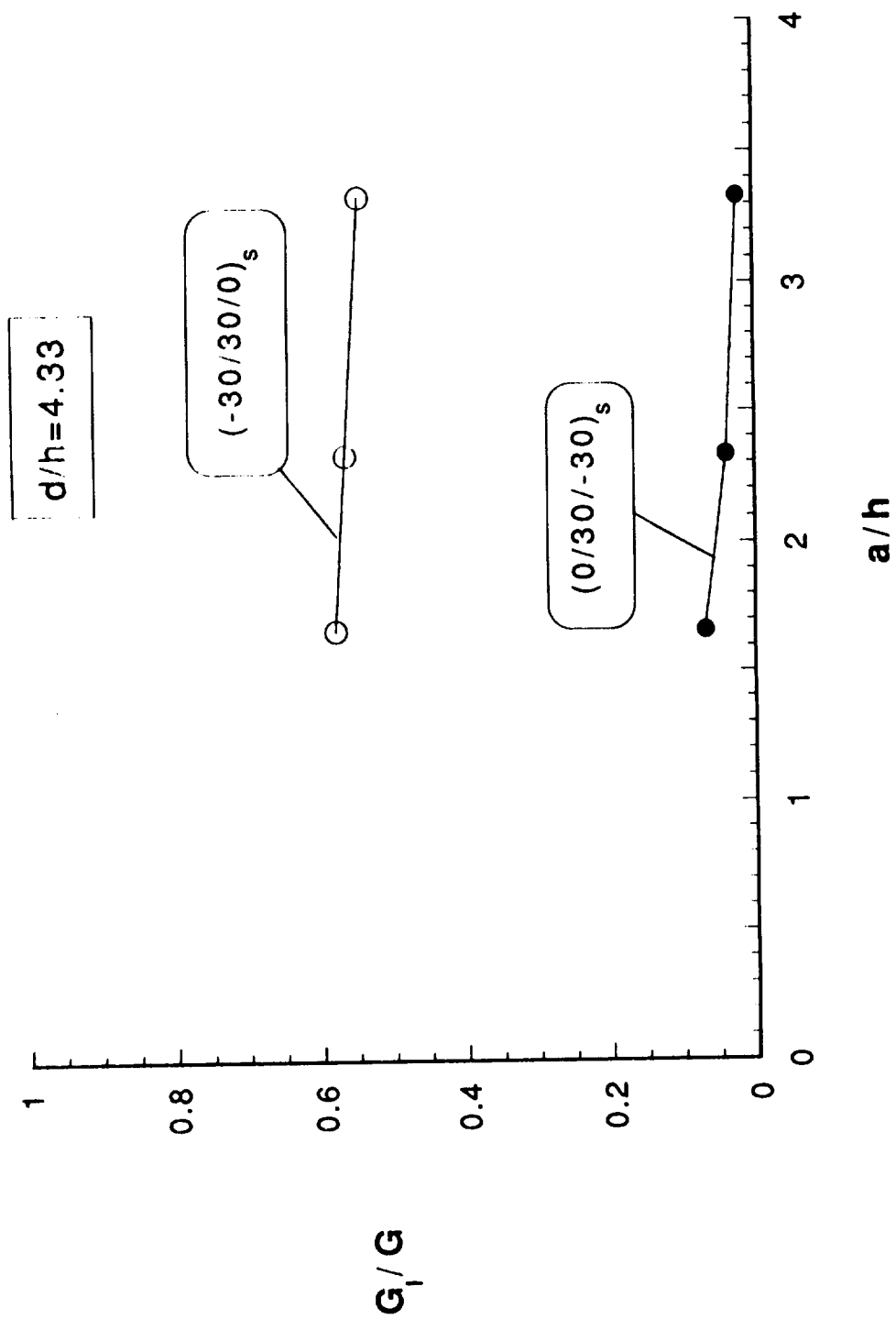


Fig.37 G_I/G near matrix crack front as a function of a/h

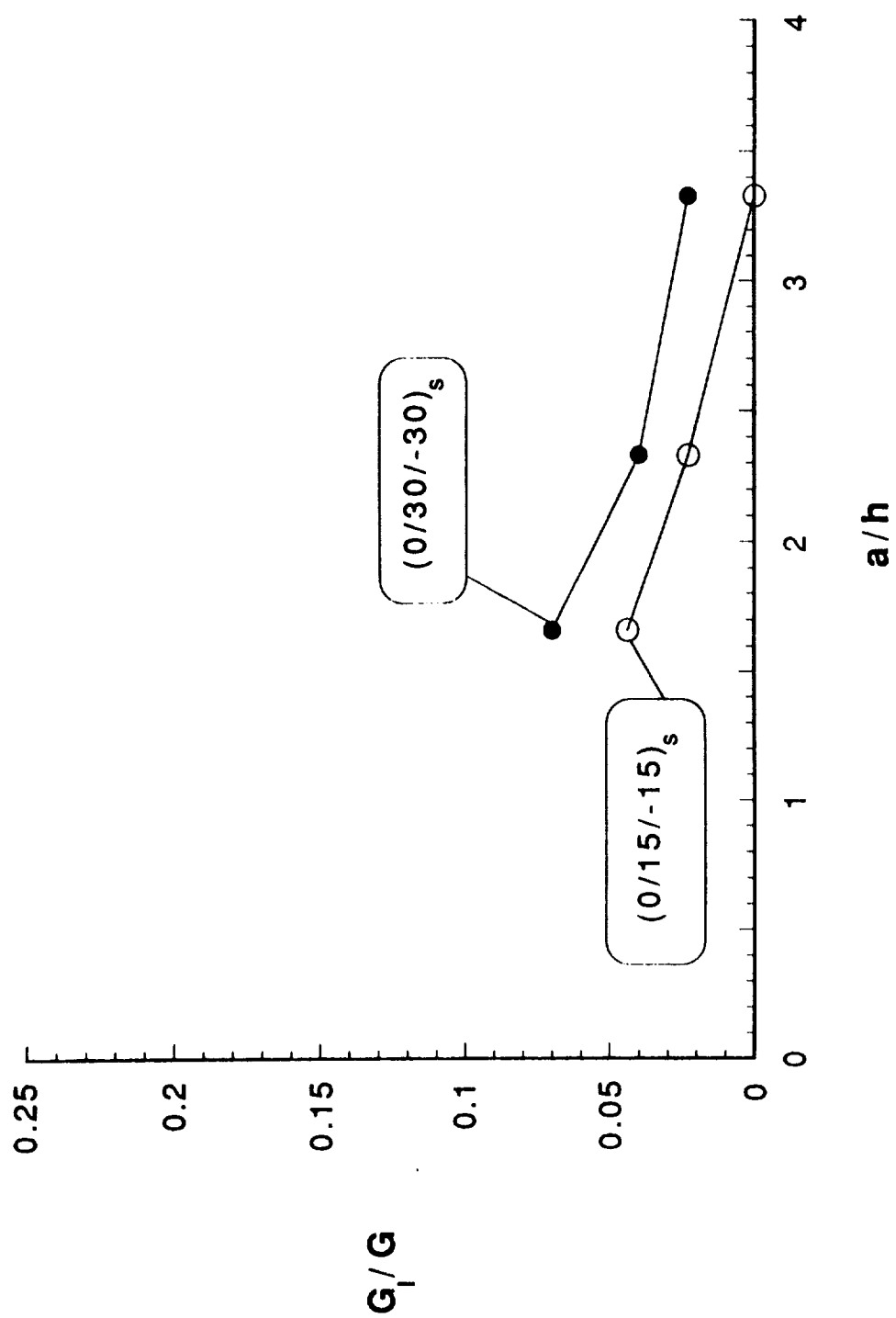


Fig.38 G_I/G near matrix crack front as a function of a/h

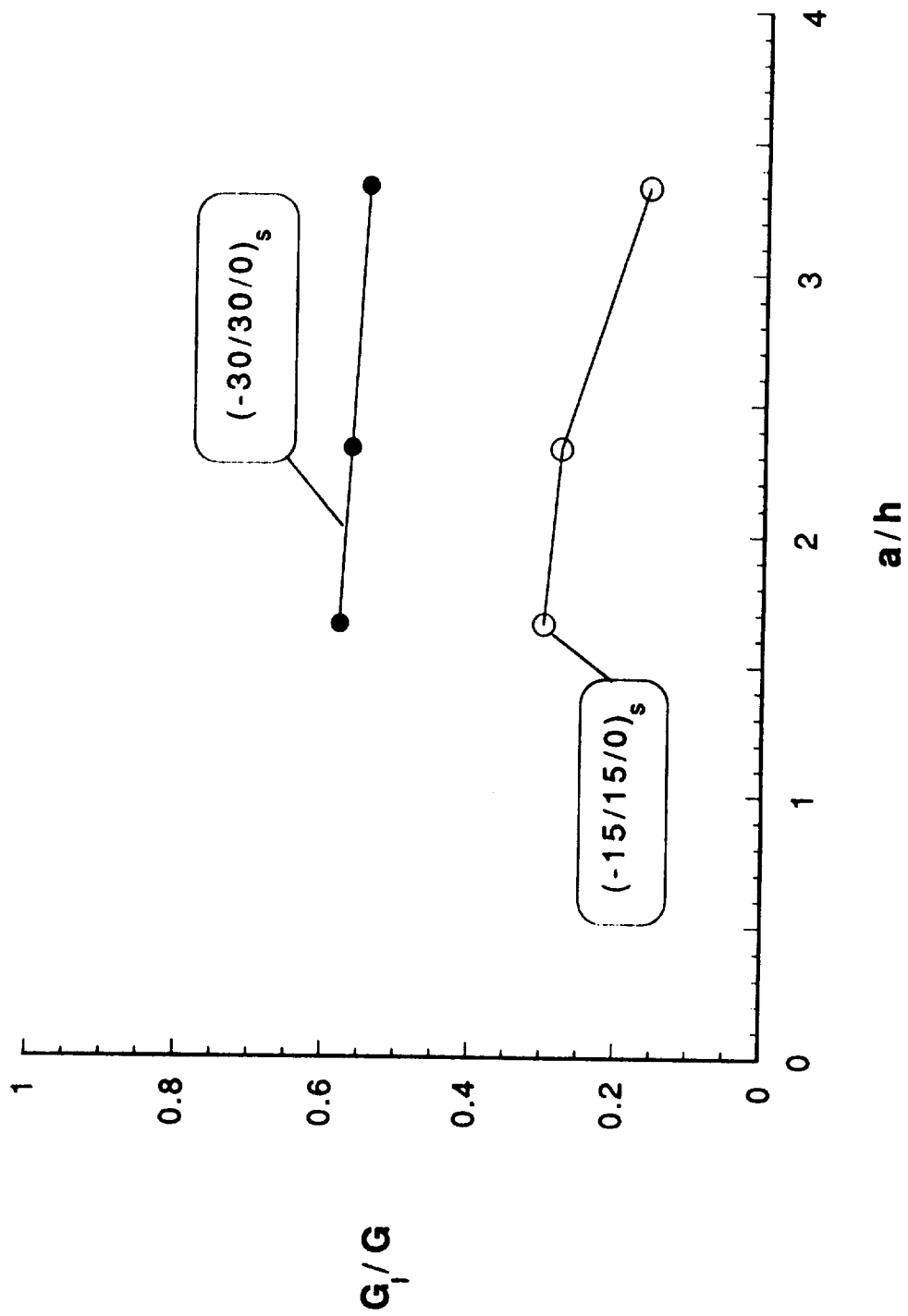


Fig.39 G_I/G near matrix crack front as a function of a/h

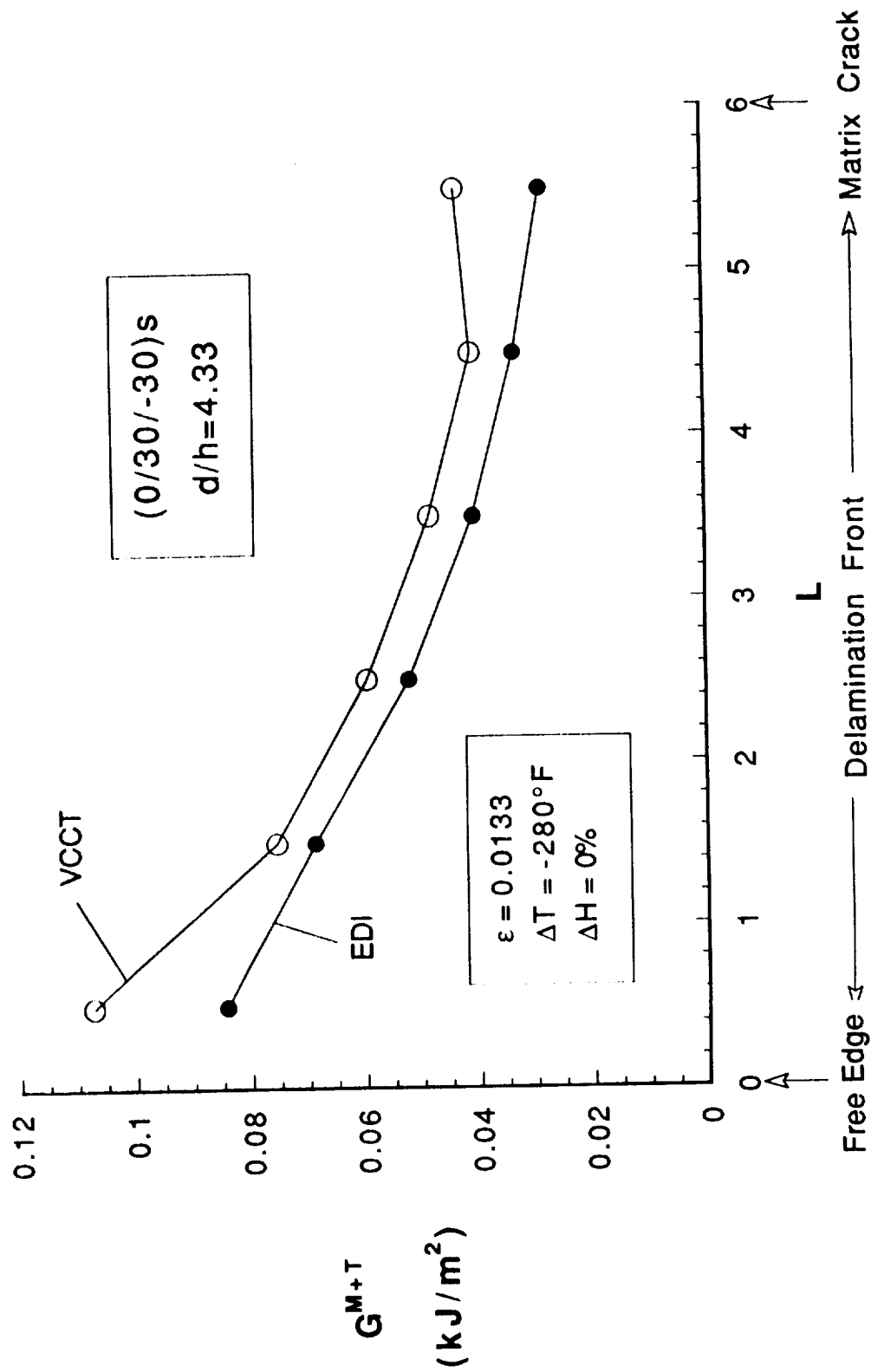


Fig.40 Total G distribution along delamination front at $a/h=3.33$ for $(0/30/-30)_s$ laminate

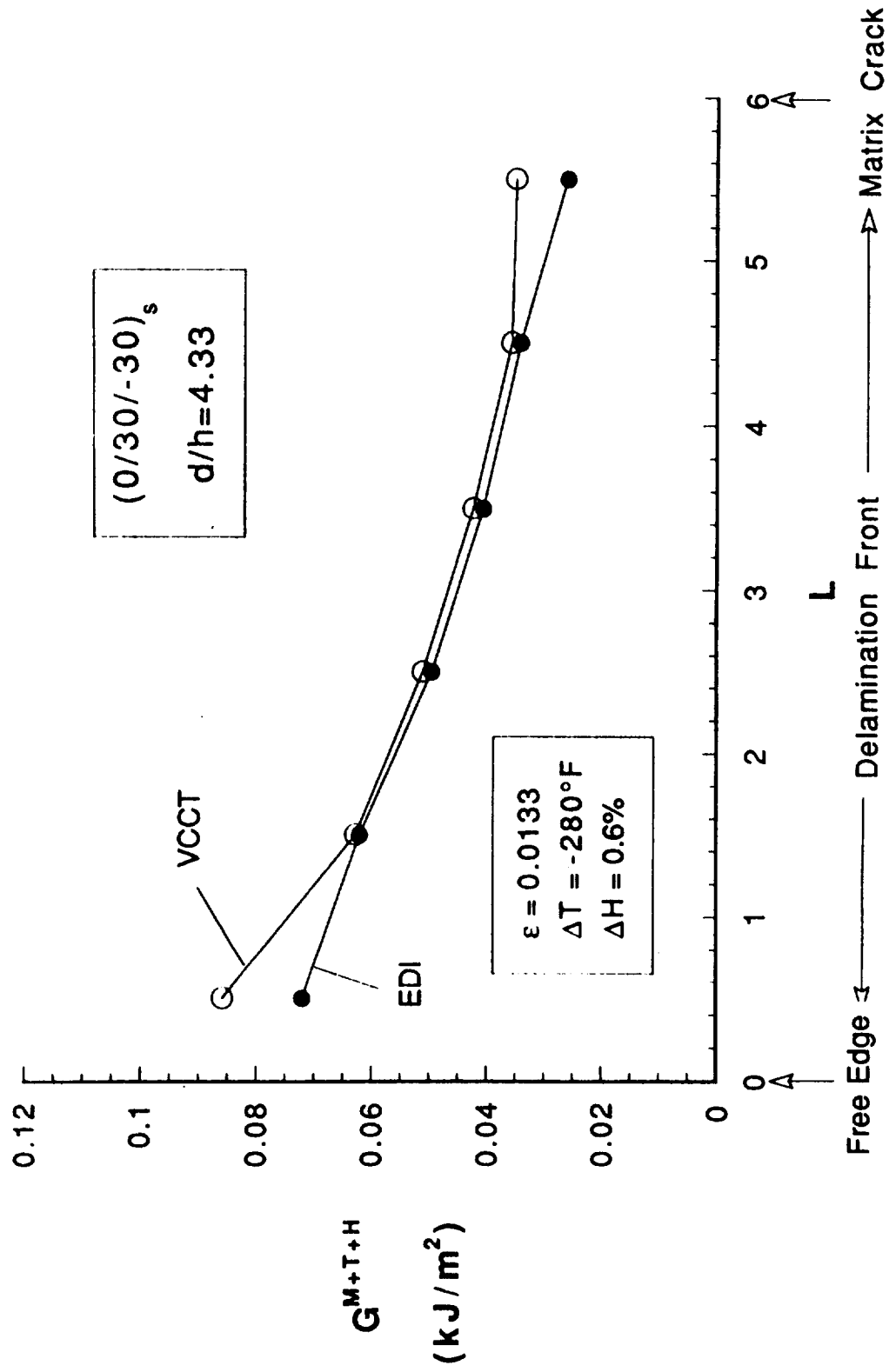


Fig.4.1 Total Gdistribution along delamination front at $a/h=3.33$ for $(0/30/-30)_s$ laminate

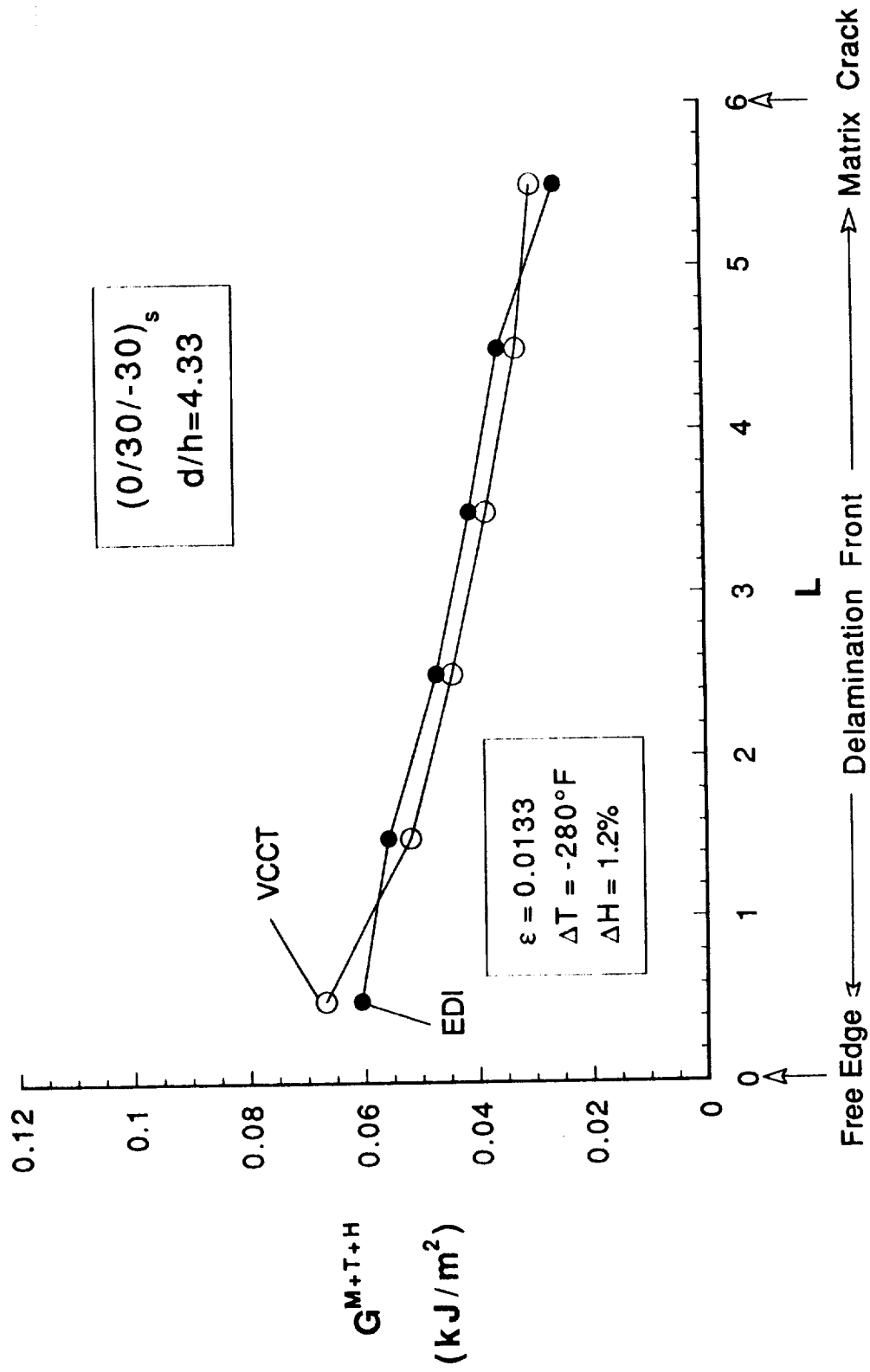


Fig.42 Total Gdistribution along delamination front at $a/h=3.33$ for $(0/30/-30)_s$ laminate

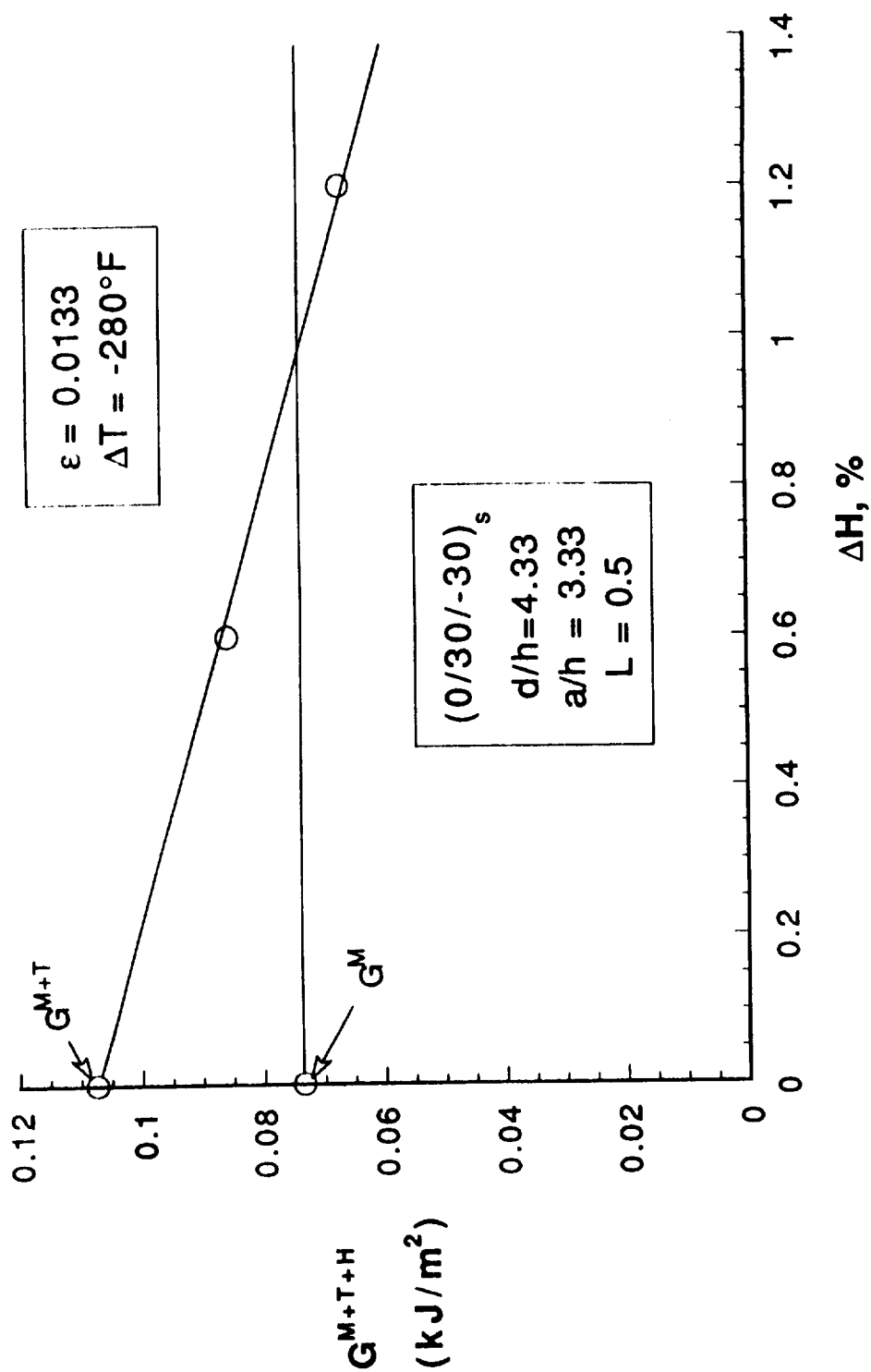


Fig.43 Total G near free edge as a function of moisture content for $(0/30/-30)_s$ laminate

REPORT DOCUMENTATION PAGE

Form Approved
OMB No 0704-0188

Public reporting burden for this collection of information is estimated to average 1 hour per response, including the time for reviewing instructions, searching existing data sources, gathering and maintaining the data needed, and completing and reviewing the collection of information. Send comments regarding this burden estimate or any other aspect of this collection of information, including suggestions for reducing this burden, to Washington Headquarters Service, Directorate for Information Operations and Reports, 1215 Jefferson Davis Highway, Suite 1204, Arlington, VA 22202-4302, and to the Office of Management and Budget, Paperwork Reduction Project (0704-0188), Washington, DC 20503.

1. AGENCY USE ONLY (Leave blank)	2. REPORT DATE November 1993	3. REPORT TYPE AND DATES COVERED Technical Memorandum
----------------------------------	---------------------------------	--

4. TITLE AND SUBTITLE Analysis of Local Delaminations Caused by Angle Ply Matrix Cracks	5. FUNDING NUMBERS WU 538-02-10-01
--	---------------------------------------

6. AUTHOR(S) Satish A. Salpekar, T. Kevin O'Brien and K. N. Shivakumar

7. PERFORMING ORGANIZATION NAME(S) AND ADDRESS(ES) NASA Langley Research Center Hampton, VA 23681-0001	8. PERFORMING ORGANIZATION REPORT NUMBER
--	--

9. SPONSORING MONITORING AGENCY NAME(S) AND ADDRESS(ES) National Aeronautics and Space Administration Washington, DC 20546-0001	10. SPONSORING MONITORING AGENCY REPORT NUMBER NASA TM 109052
---	--

11. SUPPLEMENTARY NOTES
Salpekar: Analytical Services & Materials, Inc., Hampton, VA; O'Brien: US Army Research Laboratory, Vehicle Structures Directorate, Langley Research Center, Hampton, VA; Shivakumar: North Carolina A & T State University, Greensboro, NC.

12a. DISTRIBUTION AVAILABILITY STATEMENT Unclassified - Unlimited Subject Category - 24	12b. DISTRIBUTION CODE
---	------------------------

13. ABSTRACT (Maximum 200 words)
Two different families of graphite/epoxy laminates with similar layups but different stacking sequences, (0/θ/θ)_s and (-θ/θ/0)_s were analyzed using three-dimensional finite element analysis for θ=15 and 30 degrees. Delaminations were modeled in the -θ/θ interface, bounded by a matrix crack and the stress free edge. The total strain energy release rate, G, along the delamination front was computed using three different techniques: the virtual crack closure technique (VCCT), the equivalent domain integral (EDI) technique, and a global energy balance technique. The opening fracture mode component of the strain energy release rate, G_I, along the delamination front was also computed for various delamination lengths using VCCT. The effect of residual thermal and moisture stresses on G was evaluated.

14. SUBJECT TERMS Composite material; Graphite epoxy; Delamination; Matrix Crack; Finite element analysis	15. NUMBER OF PAGES 66
	16. PRICE CODE A04

17. SECURITY CLASSIFICATION OF REPORT Unclassified	18. SECURITY CLASSIFICATION OF THIS PAGE Unclassified	19. SECURITY CLASSIFICATION OF ABSTRACT	20. LIMITATION OF ABSTRACT
---	--	---	----------------------------